Chapter 8
Polarization Bremsstrahlung on Nanostructures

8.1 PBs on Atomic Clusters in a Wide Spectral Range

In Chap. 1 of this monograph the examples of calculation of PBs of an electron on a nanocluster in the low-frequency range were given, when the photon energy is from 1 to several tens of eV [1]. Here we will consider bremsstrahlung of a relativistic electron scattered on atomic clusters in a wide frequency range with an emphasis on the role of cooperative effects in the polarization and ordinary (static) channels of the process [2].

Let us calculate the intensity of the polarization and ordinary channels of Bs of a fast charged particle on a cluster within the framework of a simple model. The main assumptions of the used approach are reduced to the first Born approximation for interaction of an IP with a target and a jelly model for the form factor of the cluster.

Further we use the quasi-classical formula for the amplitude of static (ordinary) bremsstrahlung and the approximate expression for the generalized polarizability of cluster atoms.

With the use of the standard quantum-mechanical procedure (see details in the work [3]), for the differential intensity of Bs by each of the channels normalized to the number of atoms in a cluster N the following expression can be obtained:

$$\frac{dI}{d\omega\, d\Omega_{\mathbf{n}}} = \frac{1}{N} \int_{q_{\min}}^{q_{\max}} T(q)\, dq, \tag{8.1}$$

where $\mathbf{q} = \mathbf{p}_f - \mathbf{p}_i + \mathbf{k}$ is the momentum transferred to the target from an IP, $T(q)$ is the partial intensity of Bs, $d\Omega_{\mathbf{n}}$ is the solid angle in the direction of radiation, ω, $\mathbf{k}$ are the frequency and the wave vector of a photon, $\mathbf{p}_{i,f}$ are the initial and finite momenta of an incident particle. In this section the atomic system of units $\hbar = e = m_e = 1$ is used.

V. Astapenko, *Polarization Bremsstrahlung on Atoms, Plasmas, Nanostructures and Solids*, Springer Series on Atomic, Optical, and Plasma Physics 72,
DOI 10.1007/978-3-642-34082-6_8,

The partial intensity of PBs within the framework of the used approach can be represented as

$$T_{pol}(q) = \frac{2\,Z_p^2}{\pi\,c^3\,\mathrm{v}\,q}\,S(q,\,N)\,\left|Z_{pol}(\omega,\,q)\right|^2 I\phi(q,\,\mathrm{v},\,\omega,\,\theta), \tag{8.2}$$

where Z_p is the IP charge, c is the velocity of light, v is the velocity of an IP, $S(q,\,N)$ is the structure factor of the cluster, $Z_{pol}(\omega,\,q)$ is the effective polarization charge of cluster atoms, $I\phi(q,\mathrm{v},\omega,\theta)$ is the kinematic integral appearing as a result of integration with respect to the azimuth angle of the vector $\mathbf{q}$, $\theta = \mathbf{p}_i\hat{}\mathbf{k}$ is the angle of photon emission.

It should be noted that the expression (8.2) was obtained for a range of high enough frequencies, in which $\omega >> I_a$, where I_a is the potential of ionization of atoms forming the cluster. An opposite case of low frequencies $\omega < I_a$ was considered in the work [4].

For the structure factor of the cluster we will use the following model approximation:

$$S(q,N) = N^2\,F_J^2(q,N) + N\left(1 - F_J^2(q,N)\right), \tag{8.3}$$

where

$$F_J(q,N) = 3\,\frac{j_1(q\,r(N))}{q\,r(N)} \tag{8.4}$$

is the form factor of the spherical cluster in the jelly model normalized to one atom.

$$j_1(x) = \frac{\sin x}{x^2} - \frac{\cos x}{x} \tag{8.5}$$

is the spherical first-order Bessel function, $r(N)$ is the cluster radius depending on the number of atoms N that can be calculated by the formula:

$$r(N) = r_{WS}\,\sqrt[3]{N} = \sqrt[3]{\frac{3\,N}{4\,\pi\,n_a}}, \tag{8.6}$$

where r_{WS} is the Wigner–Seitz radius, n_a is the solid-state concentration of cluster atoms.

The first summand on the right side of the Eq. 8.3 is the coherent part of the structure factor of the cluster, the second summand is its incoherent part. It should be noted that the forms factor (Eq. 8.4) is normalized to the number of atoms by the spatial Fourier transform of probability of distribution of atoms in a cluster in the jelly model:

$$w_J(r,N) = \frac{3\,N\,\Theta(r(N) - r)}{4\,\pi\,r(N)^3}, \tag{8.7}$$

where $\Theta(x)$ is the Heaviside step function. In case of a monatomic cluster the structure factor (Eq. 8.4) is equal to one.

The polarization charge of cluster atoms can be represented as

$$Z_{pol}(\omega, q) = \omega^2 \left|\alpha(\omega, q)\right| \cong \omega^2 \left|\alpha(\omega)\right| \tilde{F}_a(q), \tag{8.8}$$

where $\alpha(\omega)$ and $\tilde{F}(q)$ are the dipole polarizability and the normalized form factor of an atom. These values were calculated by the method proposed in [5]. The imaginary part of the polarizability was determined with the use of the optical theorem in terms of the cross-section of photoabsorption of an atom by the data given at the site of the Berkeley National Laboratory. Then the real part of the polarizability was restored with the use of the Kramers-Kronig relation. The atomic form factor was calculated in the Slater approximation by the formula obtained in the paper [6].

The kinematic integral included in the partial intensity of PBs (Eq. 8.2) is determined by the equation

$$I\phi(q, \mathrm{v}, \omega, \theta) = \frac{AD - BE - CD}{\left(D^2 - E^2\right)^{3/2}} + \frac{CD}{E^2\sqrt{D^2 - E^2}} - \frac{C}{E^2}, \tag{8.9}$$

where A, B, C, D, E are rather cumbersome functions of the problem parameters, the explicit form of which is given in [5].

The approximate expression for the partial intensity of ordinary Bs in the quasi-classical approximation $\varepsilon_i >> \omega$ (ε_i is the initial IP energy) and the relativistic limit ($\mathrm{v} \approx \mathrm{c}$) looks like:

$$T_{st}(q) \cong \frac{2}{3\,\pi\, c^3\, \mathrm{v}\, q}\, S(q, N) \left(\frac{Z_p}{m_p}\right)^2 Z^2 \left(1 - F_a(q)\right)^2 \frac{\left(1 - (\mathrm{v}/\mathrm{c})^2\right)\left(1 + \cos^2\theta\right)}{\left(1 - (\mathrm{v}/\mathrm{c})\,\cos\theta\right)^2}, \tag{8.10}$$

where m_p is the IP mass, Z is the charge of an atomic nucleus. It should be noted that the relative error of the formula (8.10) for nonrelativistic IP velocities does not exceed 30 %.

The above formulas describe the intensities of two Bs channels in scattering of a fast charged particle by a cluster for high enough radiation frequencies $\omega >> I_a$. We neglect the inter-channel interference summand due to different dependence of PBs and SBs amplitudes on a transferred momentum, and in the relativistic case – on a radiation angle too.

Let us use the obtained formulas for calculation of intensity of Bs by the static and polarization channels in scattering of a fast electron by polyatomic clusters.

We will characterize the cooperative effects in Bs by the following ratio:

$$\xi = \frac{dI(N)}{dI(N = 1)}, \tag{8.11}$$

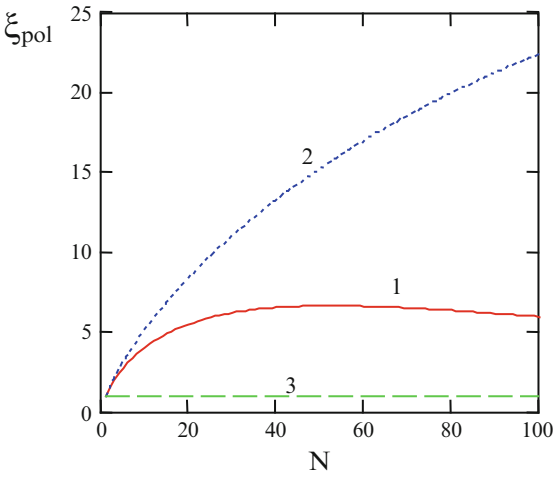

Fig. 8.1 Cooperative effects in PBs and SBs of an electron scattered by a copper cluster ($\gamma = 10$, $\hbar\omega = 1$ keV); *1* – PBs, $\theta = 1$ rad; *2* – PBs, $\theta = 0.5$ rad; *3* – SBs

where dI is the differential intensity of Bs by one of the channels normalized to the number of atoms in a cluster. In the absence of cooperative effects it is obvious that $\xi = 1$. In the opposite limiting case of constructive interference of contributions of cluster atoms to the Bs intensity we have: $\xi = \chi N$, $\chi < 1$. The coefficient χ takes into account the fact that transferred momenta essential in the process on an individual atom do not all make a considerable contribution to the coherent part of Bs on a cluster.

The dependence of the parameter ξ on the number of atoms in a copper cluster for both Bs channels is presented in Fig. 8.1. The bremsstrahlung photon energy is 1 keV, the Lorenz factor is $\gamma = 10$ ($\gamma = \left(1 - (\mathrm{v/c})^2\right)^{-1/2}$).

In case of the polarization channel the dependence $\xi(N)$ is given for two values of the radiation angle $\theta = 0.5,\ 1$ rad. From the figure it follows that cooperative effects are negligible for the static Bs channel and rather substantial for the polarization channel. The analysis shows that the value of cooperative effects in PBs grows noticeably with decreasing radiation angle. Besides, their role increases with growing IP energy and decreasing bremsstrahlung photon frequency. From the given curves and calculation data it follows that in case of the polarization channel, beginning from some value N_{sat} depending on the radiation angle and IP energy, the saturation of radiation intensity as a function of the number of atoms in a cluster takes place. The analysis shows that with decreasing radiation angle and growing IP energy the value N_{sat} grows.

For explanation of the listed regularities we will take into account the fact that, as follows from the formulas for the structure factor (Eqs. 8.3, 8.4, 8.5 and 8.6), constructive interference of contributions of different cluster atoms to the process takes place only for low enough values of the transferred momentum:

$$q < 1/r(N), \tag{8.12}$$

where $r(N)$ is the radius of the cluster (Eq. 8.6). Otherwise the structure factor of the cluster (normalized to the number of atoms) is equal to one, and cooperative effects are absent.

It is essential that the inequation (8.33) is incompatible with the condition

$$q > 1/r_a \tag{8.13}$$

defining the range of transferred momenta, in which ordinary Bs is not low in view of the obvious inequation $r(N) > r_a$ (r_a is the characteristic atomic radius). Hence a negligible value of cooperative effects in ordinary Bs on a cluster follows.

At the same time the partial amplitude of PBs is great in case of fulfilment of an inequation opposite to Eq. 8.13, so there is no analogous prohibition of cooperative effects in the polarization channel. Let us write out the expression for a minimum momentum transferred to the target from an IP, appearing in the integral (8.1):

$$q_{\min}(\omega, \mathrm{v}, \theta) = \frac{\omega}{\mathrm{v}} \left(1 - \frac{\mathrm{v}}{c} \cos\theta\right). \tag{8.14}$$

Following from the condition of essentiality of cooperative effects

$$q_{\min} < 1/r(N) \tag{8.15}$$

and the formula (8.6) for the cluster radius is the expression for the saturating value of the number of atoms in a cluster N_{sat}:

$$N_{sat} = \frac{4\,\pi\, n_a\, \mathrm{v}^3}{3\,\omega^3 \left(1 - \frac{\mathrm{v}}{\mathrm{c}} \cos\theta\right)^3}. \tag{8.16}$$

Following from Eq. 8.16 is the strong dependence of the value N_{sat} on the radiation angle and IP energy in the relativistic case. For example, for the parameters of Fig. 8.1 we have: $N_{sat}(\theta = 1\ rad) = 27$ and $N_{sat}(\theta = 0.5\ rad) = 1,312$.

The influence of cooperative effects on the angular dependence of PBs on a cluster is demonstrated by Fig. 8.2. Shown in this figure is the PBs intensity normalized to its value at a zero angle as a function of the radiation angle for different numbers of atoms in a copper cluster, including a monatomic case, at the photon energy of 5 keV and a Lorenz factor of 10.

It is seen that the angular distribution of PBs with growing number of atoms is narrowed, and its dependence on an angle in the limit of high values of the number N becomes nonmonotonic. This nonmonotonicity disappears in the nonrelativistic case with decreasing radiation frequency and grows with increasing number of atoms.

It should be noted that the said dependences in the angular distribution of PBs on clusters can be found experimentally only for heavy IP. In case of light IP (electron, positron), at small radiation angles the static channel prevails, cooperative effects in which are low.

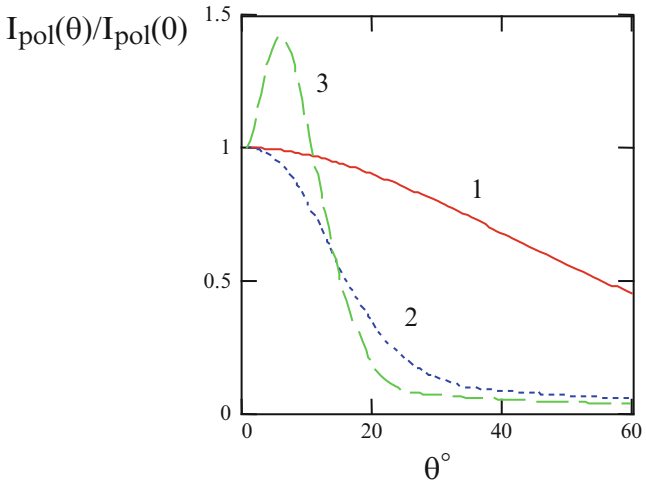

Fig. 8.2 The angular dependence of the normalized intensity of PBs of an electron on an individual atom (Eq. 8.22) and a copper cluster: N = 100 (Eq. 8.23), N = 1,000 (Eq. 8.24); $\hbar\omega = 5$ keV, $\gamma = 10$

To describe the relative contribution of PBs to the process, let us introduce the R-factor according to the equation:

$$R = \frac{dI_{pol}}{dI_{st}}. \tag{8.17}$$

The angular dependence of the R-factor of an electron with $\gamma = 10$ for a photon energy of 1 keV and different numbers of atoms in a copper cluster is presented in Fig. 8.3. It is seen that with increasing number of atoms the role of PBs grows. For example, for a monatomic case the angle, at which the intensities of PBs and SBs become equal, is 30°, and for $N = 100$ this angle is 10°.

Figure 8.4 demonstrates the influence of cooperative effects on the relative contribution of the polarization channel to emission of a fast electron ($\gamma = 10$) scattered by a copper cluster at different energies of a bremsstrahlung photon and a radiation angle of 15°.

The growth of the R-factor with increasing number of electrons in a cluster goes to saturation more fast for high photon energies according to the formula (8.16) for the value N_{sat}. Following from this figure is the strong dependence of the role of polarization effects on the cluster size, especially in the low-frequency range.

The condition of essentiality of cooperative effects in the spectrum of PBs on a cluster can be obtained from the inequation (8.15) in view of the explicit expression for the minimum momentum transferred to the target (Eq. 8.14). It looks like:

$$\omega < \omega_{\max} = \sqrt[3]{\frac{4\pi n_a}{3N}} \frac{\mathrm{v}}{1 - \frac{\mathrm{v}}{\mathrm{c}}\cos\theta}. \tag{8.18}$$

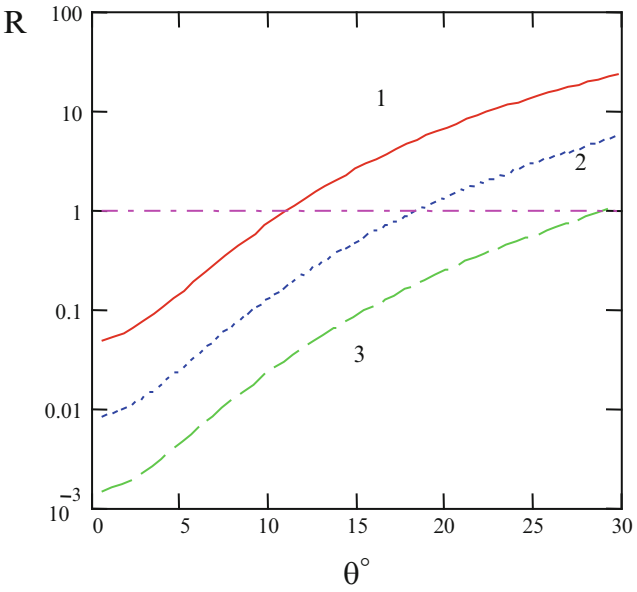

Fig. 8.3 The angular dependence of the *R*-factor for different numbers of atoms in a copper cluster including a monatomic case: $\hbar\omega = 1$ keV, $\gamma = 10$, *1* – N = 100, *2* – N = 10, *3* – N = 1

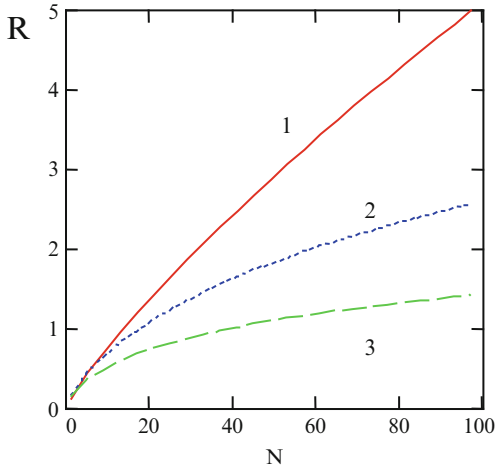

Fig. 8.4 The dependence of the *R*-factor on the number of atoms in a copper cluster for different frequencies *1* – $\hbar\omega = 500$ *eV*, *2* – $\hbar\omega = 2$ *keV*, *3* – $\hbar\omega = 3$ *keV*; $\gamma = 10$, $\theta = 15°$

For frequencies more than ω_{max} cooperative effects in Bs on a cluster are low.

In the nonrelativistic limit v<<c the maximum frequency of manifestation of cooperative effects does not depend on the radiation angle and is:

$$\omega_{\max}^{nrel} = \frac{\mathrm{v}}{r_{WS}\sqrt[3]{N}}. \tag{8.19}$$

The value of the Wigner–Seitz radius for metal clusters varies within $r_{WS} = 2 \div 4$, so the characteristic value of frequency (Eq. 8.19) for a mid-size cluster and an IP velocity about 10 a.u. is 1 a.u.

It should be noted that in the frequency a range $\omega < 1$ a.u. the calculation model used here becomes inadequate since then the dynamic polarizability of the cluster will be to a great extent defined by collective excitations of the cluster electrons. Such a situation for a nonrelativistic IP was considered in the work [7].

In the relativistic limit $\gamma >> 1$ it is convenient to represent the formula (8.18) in the form:

$$\omega_{\max} = \frac{1}{r_{WS}\sqrt[3]{N}} \frac{2\gamma^2}{4\gamma^2 \sin^2(\theta/2) + 1} \tag{8.20}$$

clearly demonstrating the dependence of the maximum frequency $\omega_{\max}$ on the IP energy. From the Eq. 8.20 it follows that in contrast to the nonrelativistic case, in the relativistic limit the influence of cooperative effects on the PBs spectrum is essentially defined by the angle of photon emission. For small angles and high values of the Lorenz factor of an IP the maximum frequency of manifestation of cooperative effects in PBs can reach high values. However, in this case it should be remembered that in the angular range $\theta < \gamma^{-2}$ in Bs of an electron (positron) the static channel prevails. So the question about a role of cooperative effects in the spectrum of Bs of a light charged particle on a cluster should be decided in view of concrete values of problem parameters. At the same time for Bs of heavy charged particles, when SBs is negligible, the spectral restriction on the role of cooperative effects in the relativistic a case is given by the frequency of Eq. 8.20.

The dependence of the spectrum of PBs on a copper cluster consisting of ten atoms on the IP energy is presented in Fig. 8.5 for a radiation angle of 0.5 rad.

It is seen that with growing Lorenz factor the intensity of radiation increases, and the maximum of the spectral dependence is shifted to the region of high frequencies. These changes are most pronounced in going from fast, but nonrelativistic IP to weakly relativistic particles. With further growth of the Lorent factor the spectrum of PBs on a cluster varies not so appreciably. With decreasing radiation angle the spectrum of PBs of relativistic IP is found to be more pulled into the region of high frequencies according to the formula (8.20), following from which is also the decrease of the maximum frequency with growing number of atoms in a cluster.

The intensity of total Bs and PBs in scattering of a nonrelativistic electron on a copper cluster and an individual atom as a function of the IP velocity is shown in Fig. 8.6 for the radiation angle $\theta = 1$ rad and the photon energy $\hbar\omega = 200$ eV. It is seen that in the nonrelativistic case there is the optimum value of the electron velocity $\mathrm{v}_{\mathrm{opt}}$, at which the intensity of PBs on a cluster is maximum. The dependence of this optimum velocity on the problem parameters is given by the expression:

$$\mathrm{v}_{\mathrm{opt}} = \omega r(N). \tag{8.21}$$

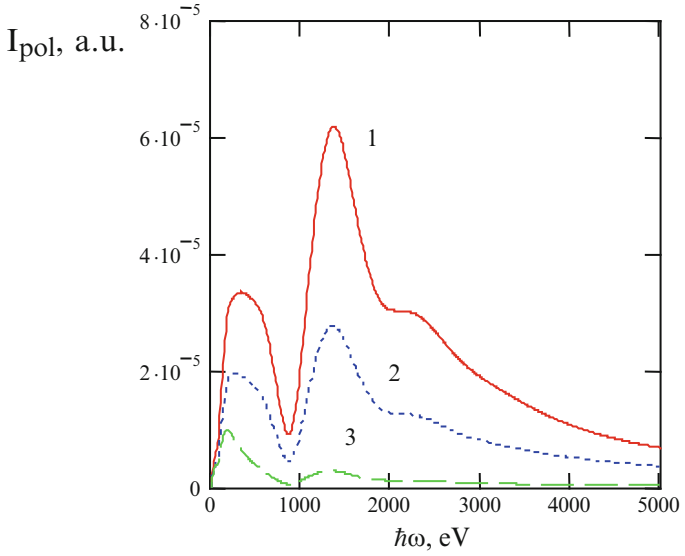

Fig. 8.5 The spectrum of PBs on a copper cluster (N = 10) for different values of the Lorentz factor and a radiation angle of 0.5 rad: *1* – $\gamma = 10^2$, *2* – $\gamma = 10$, *3* – $\gamma = 1.1$

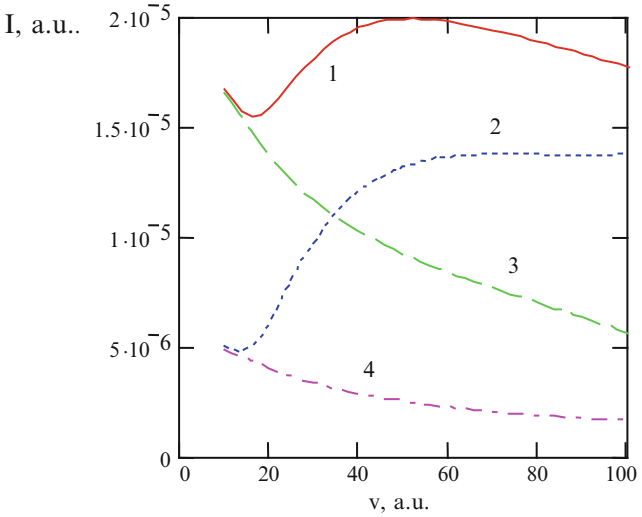

Fig. 8.6 The dependence of the Bs and PBs intensity on the electron velocity in the nonrelativistic case for a copper cluster (N = 20) and an individual atom, $\hbar\omega = 200$ eV, $\theta = 1$ rad. *1* – total Bs (N = 20), *2* – PBs (N = 20), *3* – total Bs (N = 1), *4* – PBs (N = 1)

In case of the process on an individual atom the cluster radius in Eq. 8.21 should be replaced by the characteristic atomic radius r_a. The given formula can be obtained with the use of the expression for the minimum transferred momentum (Eq. 8.14) in the case v<<c.

From the Eq. 8.21 it follows that with decreasing frequency and size of a cluster the value of the optimum velocity decreases. In particular, for the process on an individual atom and the photon energy $\hbar\omega = 200\,\text{eV}$ the value v_{opt} lies beyond the range of applicability of the Born approximation, so the velocity dependence of the Bs and PBs intensity looks like a monotonically decreasing curve. With growing number of atoms in a cluster the value of the optimum velocity increases as seen from the formulas (8.21) and (8.6).

With decreasing radiation angle the maximum in the velocity dependence of the Bs intensity disappears, and for PBs it becomes less pronounced. This is connected, on the one hand, with increasing contribution of the static channel to the process (see the formula (8.10)), and on the other hand, with growing value of the minimum transferred momentum (Eq. 8.14).

Figure 8.6 demonstrates the disappearance of cooperative effects with decreasing IP velocity: for the given photon energy (200 eV) the total Bs and PBs on a cluster and one atom coincide in the limit of low velocities.

In the high-frequency range the velocity dependence of the PBs intensity becomes monotonically increasing, which is connected with the natural restriction on the optimum IP velocity: $v_{opt}<137$. The monotonically increasing dependence of the PBs intensity on the IP energy is characteristic also for the relativistic case (with the exception of low frequencies not considered here).

Based on the analysis carried out in this section, it is possible to draw a conclusion about the essentiality of cooperative effects in Bs of a fast (including relativistic) charged particle scattered by a polyatomic cluster in a wide range of frequencies. These effects caused by constructive interference of the contributions of atoms to the process by the polarization channel result in nonlinear growth of the PBs intensity as a function of the number of atoms in a cluster. At the same time for the static Bs mechanism the contribution of different atoms to radiation is incoherent, which is caused by the smallness of impact parameters, on which SBs is formed.

It is shown that cooperative effects result in significant modification of the main characteristics of Bs on a cluster in comparison with a monatomic case. For example, in the high-frequency range with growing number of atoms the pattern of PBs is narrowed, and for large enough clusters the angular dependence of PBs of relativistic particles becomes nonmonotonic: a maximum appears with nonzero radiation angles.

With growing IP energy the maximum of the spectral distribution of PBs on a cluster is shifted to the region of high frequencies. The form of the high-frequency part of the spectrum in the relativistic case strongly depends on the radiation angle. With reduction of this angle the Bs intensity decreases with growing frequency much more slowly than for wide angles.

The analysis of the Bs intensity as a function of the IP velocity has shown that in the nonrelativistic case this dependence can be of different nature: from monotonically increasing to monotonically decreasing. In the relativistic limit the PBs intensity monotonically increases with IP energy. In the limit of low IP velocities the role of cooperative effects in Bs on a cluster becomes negligible.

The obtained results can be used in interpretation of experimental data on Bs of fast charged particles on clusters in the range of high enough photon energies.

8.2 PBs on Metal Nanospheres in a Dielectric Matrix

Metal nanoparticles of noble metals find use as nanomarkers for biological objects, for investigation of behavior of chemical and biological processes, as sensors for local optical environmental monitoring, for electrical control of light switching, for measurement of an electric charge, etc. [8]. In the said applications, as a rule, scattering of electromagnetic radiation in the spectral range corresponding to excitation of surface plasmons (the photon energy $\hbar\omega = 1 \div 4$ eV) is used.

Polarization bremsstrahlung (PBs) is a fundamental radiative process that can be interpreted as the conversion of the eigenfield of a charged particle on target electrons to a propagating electromagnetic wave [9]. Following from this interpretation is a possibility (by analogy with ordinary radiation) to use PBs for substance spectroscopy, in particular, for determination of parameters of metal nanoparticles.

In recent years works have appeared that are dedicated to the study of PBs as a basic process for nanomaterial diagnostics. For example, in the paper [10] a possibility to use this process for determination of a fullerene structure on the basis of calculation of a target form factor was discussed. PBs spectroscopy for diagnostics of polycrystalline and fine-grained media in the more general context of modification of the energy dispersion method was considered in the work [11]. We believe that PBs spectroscopy has also considerable promise as a physical method for metal nanosphere diagnostics.

8.2.1 General Formulas

In the Born approximation for interaction of an incident particle (IP) with a target in a dielectric medium the differential PBs cross-section is given by the expression [2] (in this section we use the Gaussian system of units):

$$\frac{d\sigma^{PB}}{d\omega\, d\Omega_{\mathbf{k}}} = \frac{2}{\pi}\frac{\omega^3}{c^3}\frac{e_p^2}{\hbar\,\mathrm{v}^2}\int\limits_{q_{\min}}^{q_{\max}} |\,\alpha(\omega,q)|^2\, I_\phi(q,\mathrm{v},\omega,\theta)\,\frac{dq}{q}, \tag{8.22}$$

where $d\Omega_{\mathbf{k}}$ is the element of a solid angle in the direction of radiation, c is the velocity of light, e_p is the IP charge, v is the IP velocity, $\alpha(\omega, q)$ is the generalized dynamic polarizability of the target, $\mathbf{k} = \sqrt{\varepsilon_m}\,(\omega/c)\,\mathbf{s}$ is the wave vector of a bremsstrahlung photon in a medium with the dielectric permittivity ε_m, θ is the angle between the

electron velocity vector and the wave vector of a bremsstrahlung photon (the radiation angle). The value $\mathbf{q} = \left(\mathbf{p}_f - \mathbf{p}_i + \mathbf{k}\right)/\hbar$ is the wave vector transferred from an IP to the target ($\mathbf{p}_{i,f}$ are the initial and finite momenta of an IP). The limits of integration on the right side of the Eq. 8.22 are $q_{\min} = (1 - (\mathrm{v}/\tilde{c})\cos\theta)(\omega/\mathrm{v})$, $q_{\max} = 2\mu\mathrm{v}/\hbar$, $\tilde{c} = c/\sqrt{\varepsilon_m}$ is the velocity of light in a medium. The dimensionless kinematic integral $I_\phi(q, \mathrm{v}, \omega, \theta)$ appearing in the formula (8.22) is determined by the equation

$$I_\phi(q, \mathrm{v}, \omega, \theta) = \frac{q^3\,\mathrm{v}}{2\pi}\int d\Omega_{\mathbf{q}}\,\delta(\omega - \mathbf{kv} + \mathbf{qv})\,\frac{\left[\mathbf{s}, \omega\,\varepsilon_m\,\mathbf{v}/c^2 - \mathbf{q}\right]^2}{\left(\mathbf{q}^2 - 2\,\mathbf{k}\,\mathbf{q}\right)^2}, \tag{8.23}$$

where $\mathbf{s}$ is the unit vector in the direction of photon emission. The solid-angle integral of the wave vector transferred to the target in the determination (8.23) can be calculated in elementary functions [5]. We do not give here a corresponding expression because of its cumbersomeness.

In the multiplicative approximation that well works for multielectron systems [12] the equation is true

$$\alpha(\omega, \mathbf{q}) = \alpha(\omega)\,\tilde{F}(q), \tag{8.24}$$

where $\alpha(\omega)$ is the dynamic polarizability, $\tilde{F}(q)$ is the normalized form factor of the target ($\tilde{F}(0) = 1$). Substituting the relation (8.24) in the formula (8.22) and using the expression for the radiation scattering cross-section in terms of the target polarizability

$$\sigma_{scat}(\omega) = \frac{8\pi}{3}\left(\frac{\omega}{c}\right)^4 |\alpha(\omega)|^2, \tag{8.25}$$

we find the representation of the cross-section of PBs on an isolated target in terms of the radiation scattering cross-section

$$\frac{d\sigma^{PB}}{d\omega\,d\Omega_{\mathbf{k}}} = \frac{3}{4\pi^2}\frac{c}{\mathrm{v}^2}\frac{e_p^2}{\hbar\omega}\,\sigma_{scat}(\omega)\int\limits_{q_{\min}}^{q_{\max}} \tilde{F}^2(q)\,I_\phi(q, \mathrm{v}, \omega, \theta)\,\frac{dq}{q}. \tag{8.26}$$

The convenient use of the expression (8.26) with regard to the analysis of PBs on metal nanospheres in a range of photon energies of 1–5 eV consists in the fact that the scattering cross-section $\sigma_{scat}(\omega)$ can be calculated using the Mie theory [13]. Within the framework of this theory the cross-section of radiation scattering by a metal sphere of the radius r_s placed in a dielectric medium looks like

$$\sigma_{scat}^{(Mie)}(\omega) = \frac{2\pi c^2}{\varepsilon_m\,\omega^2}\sum_{n=1}^{\infty}(2n+1)\left\{|a_n(x, mx, m)|^2 + |b_n(x, mx, m)|^2\right\}, \tag{8.27}$$

where $x = k\,r_s = \sqrt{\varepsilon_m}\,\frac{\omega}{c}\,r_s$ and $m = \sqrt{\varepsilon_s(\omega)/\varepsilon_m}$ are the parameters of the Mie theory, $\varepsilon_s(\omega)$ is the dielectric permittivity of the nanosphere material. The expansion coefficients a_n and b_n are

$$a_n(x,y,m) = \frac{\psi'_n(y)\,\psi_n(x) - m\,\psi'_n(x)\,\psi_n(y)}{\psi'_n(y)\,\zeta_n(x) - m\,\zeta'_n(x)\,\psi_n(y)}, \tag{8.28}$$

$$b_n(x,y,m) = \frac{m\,\psi'_n(y)\,\psi_n(x) - \psi'_n(y)\,\psi'_n(x)}{m\psi'_n(y)\,\zeta_n(x) - \zeta'_n(x)\,\psi_n(y)}, \tag{8.29}$$

$$\psi_n(z) = z\,j_n(z) = \sqrt{\frac{\pi\,z}{2}}J_{n+1/2}(z), \tag{8.30}$$

$$\zeta_n(z) = z\,h_n^{(1)}(z) = \sqrt{\frac{\pi\,z}{2}}H_{n+1/2}^{(1)}(z) \tag{8.31}$$

are the functions coined by Debye; $j_n(z), h_n^{(1)}(z)$ are the spherical Bessel and Hankel functions, $J_{n+1/2}(z)$ and $H_{n+1/2}^{(1)}(z)$ are the Bessel and Hankel functions.

The formula for the normalized form factor of a spherical target looks like [2]

$$\tilde{F}_s(q) = 3\,\frac{j_1(q\,r_s)}{q\,r_s}. \tag{8.32}$$

From this equation it follows in particular that $\tilde{F}_s(q=0) = 1$ and $\tilde{F}_s(q > 4/r_s) < 0.01$.

8.2.2 Results and Discussion

The spectral dependences of the PBs cross-section are presented in Fig. 8.7 for different nanosphere radii and in Fig. 8.8 for different velocities of an incident electron; the radiation angle in these figures is taken equal to 30°.

The maximum of the spectral dependence of the PBs cross-section shown in Fig. 8.7 is caused by excitation of a plasmon on the surface of the metal sphere under the action of the electric field of a scattered electron. From this figure it is seen that with increasing nanosphere radius the position of the spectral maximum of the PBs cross-section is shifted to the region of lower photon energies, and its width increases.

An analogous dependence takes place for the cross-section of radiation scattering by metal nanospheres [8], which is caused by a change of the resonance frequency of a surface plasmon ω_{res} with changing radius of the sphere. Really,

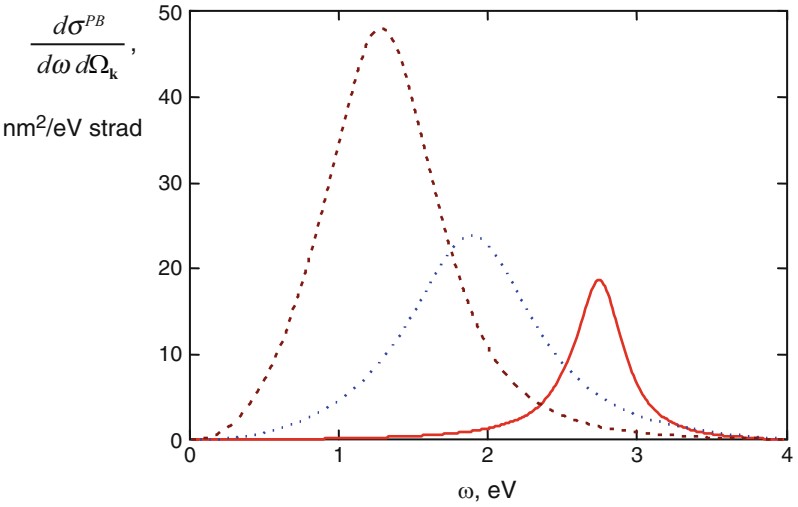

Fig. 8.7 The differential PBs cross-section for electron scattering by silver spheres with different radii in glass: *solid line* – $r_s = 30$ nm, *dotted line* – $r_s = 60$ nm, *dashed line* – $r_s = 90$ nm, $\theta = \pi/6$, $v = 50$ a.u.

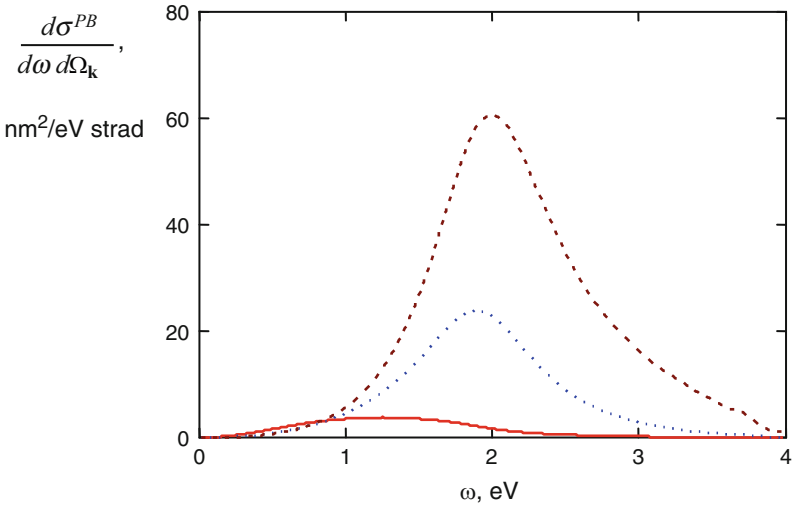

Fig. 8.8 The differential PBs cross-section for electrons with different velocities scattered by a silver sphere in glass: *solid line* – $v = 20$ a.u., *dotted line* – $v = 50$ a.u., *dashed line* – $v = 90$ a.u., $\theta = \pi/6$, $r_s = 60$ nm

the expression for the resonance frequency of a dipole plasmon on the sphere surface looks like

$$\omega_{res} \simeq \sqrt{\frac{\omega_p^2}{\varepsilon_\infty + 2\,\varepsilon_m} - \gamma^2}, \tag{8.33}$$

where ω_p is the plasma frequency of electrons of the sphere substance, γ is the damping constant of a surface plasmon, $\varepsilon_\infty - 1$ is the contribution of bound electrons to the dielectric permittivity of the metal. For large enough radii ($r_s > 30$ nm in case of a silver sphere) the damping constant becomes proportional to the cubed radius of the sphere $\gamma \propto r_s^3$, which defines a shift of the maximum of the radiation scattering and PBs cross-sections with increasing radius of the metal sphere.

Shown in Fig. 8.8 is the PBs cross-section as a function of the photon energy for different electron velocities and a silver sphere radius of 60 nm, the radiation angle is 30°. It is seen that for specified values of parameters the PBs cross-section with increasing electron velocity increases, and its spectral maximum is shifted to the region of higher frequencies. For small nanosphere radii $r_s < 20$ nm on the spectral curve of the PBs cross-section additional maxima appear that are caused by excitation of quadrupole and octupole surface plasmons.

It is seen that with approach of the electron velocity to the velocity of light in the glass matrix $\mathrm{v}* = \tilde{c} = c/\sqrt{\varepsilon_m} \simeq 91.33$ a.u. the velocity dependence of the PBs cross-section has singularity. Physically the said singularity corresponds to a possibility of radiation by an electron of a propagating electromagnetic field in a medium without scattering by a nanosphere. Besides, following from Fig. 8.9 is the presence of maxima on the velocity dependence of the PBs cross-section for small enough metal sphere radii. The value of electron velocity $\mathrm{v}_{\max}$ corresponding to these maxima decreases with decreasing radius according to the relation $\mathrm{v}_{\max} \propto \omega\, r_s$.

Oscillations of the PBs cross-section in Fig. 8.9 at low electron velocities arise due to the contribution to the process of transferred wave vectors of high magnitude: $q > 4/r_s$, when oscillations of the target form factor (Eq. 8.32) as functions of the argument $x = q\, r_s$ take place.

The dependence of the differential PBs cross-section on the nanosphere radius for different energies of a bremsstrahlung photon is demonstrated in Fig. 8.10 for an electron velocity of 50 a.u. and a radiation angle of 90°. It follows from Fig. 8.10 that with increasing photon energy the optimum radius of a nanoparticle, at which the PBs cross-section is maximum, decreases. In this case it turns out that the greatest value of the cross-section at the maximum of the radius dependence is reached for $\hbar\,\omega = 2.8$ eV.

Figure 8.11 demonstrates the narrowing of the angular dependence of the normalized PBs cross-section with increasing nanosphere radius for an IP velocity close to the velocity of light in a medium: $\mathrm{v} \to \tilde{c}$. The normalization of the cross-section was carried out to its value at a zero radiation angle. It is seen from this figure that for small nanosphere radii ($r_s = 10$ nm) the angular dependence of the PBs cross-section practically coincides with the angular dependence of linear dipole

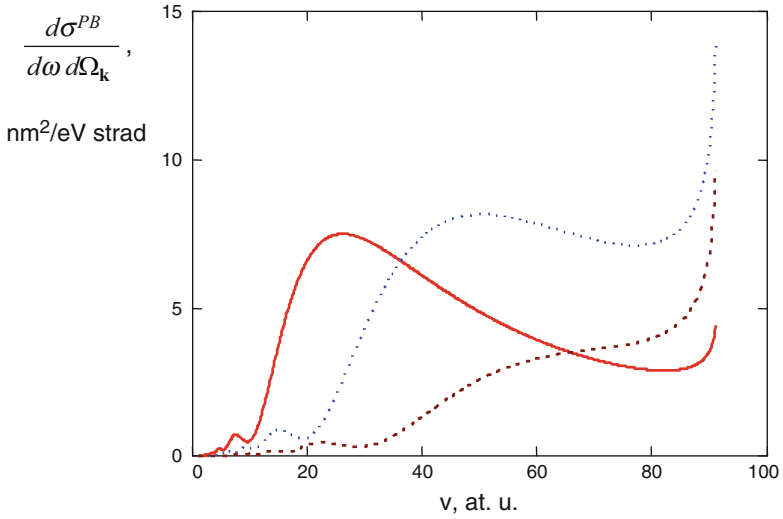

Fig. 8.9 The PBs cross-section for electron scattering by a silver sphere in glass as a function of the electron velocity for $\theta = \pi/2, \hbar\omega = 2.8$ eV. *Solid line* – $r_s = 20$ nm, *dotted line* – $r_s = 40$ nm, *dashed line* – $r_s = 60$ nm

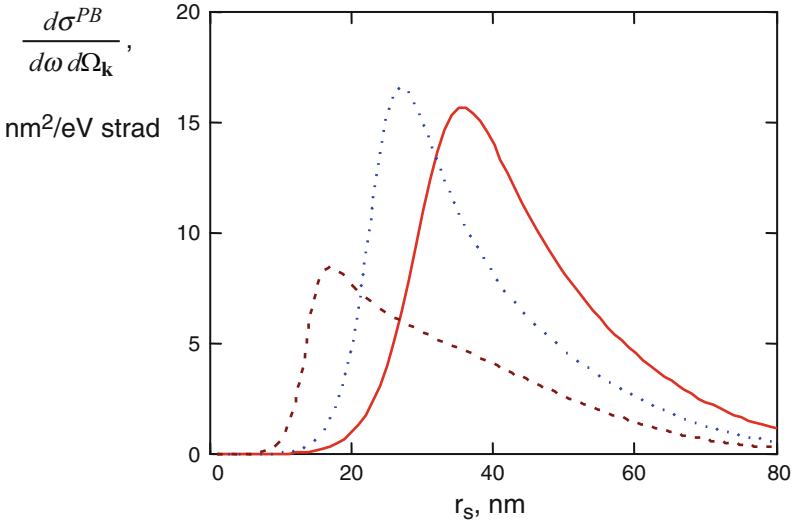

Fig. 8.10 The PBs cross-section for electron scattering by a silver sphere in glass as a function of the sphere radius for v = 50 a.u., $\theta = \pi/2$. *Solid line* – $\hbar\omega = 2.6$ eV, *dotted line* – $\hbar\omega = 2.8$ eV, *dashed line* – $\hbar\omega = 3.0$ eV

radiation. For lower electron velocities the effect of narrowing of the angular PBs distribution also takes place, though it is not so pronounced.

Thus in this section polarization bremsstrahlung on metal spheres in a dielectric medium is investigated theoretically with the use of the Mie theory of light scattering.

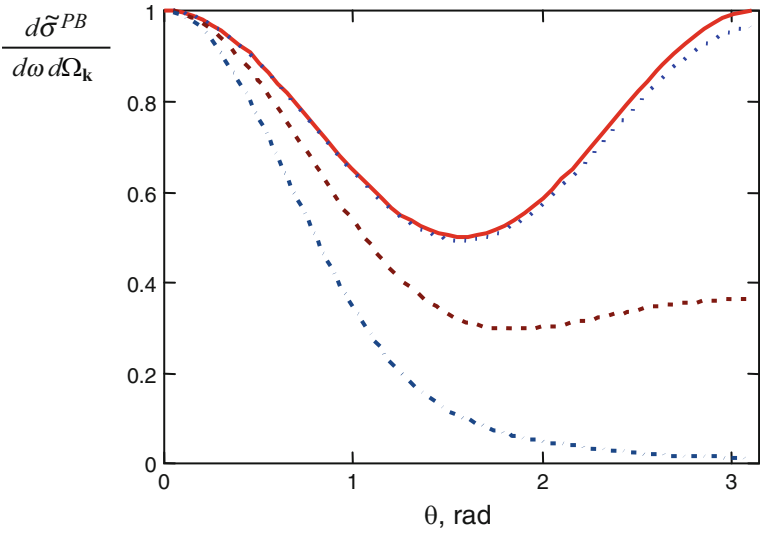

Fig. 8.11 The angular dependence of the normalized PBs cross-section for electron scattering by a silver sphere in glass for $v = 91$ a.u., $\hbar\omega = 2.8$ eV. *Solid line* is the dipole dependence $(1 + \cos^2\theta)/2$, *dotted line* $-r_s = 10$ nm, *dashed line* $-r_s = 50$ nm, *dash-and-dot line* $-r_s = 90$ nm

The spectral-angular distribution of PBs is calculated in the vicinity of a surface plasmon resonance for different radii of nanospheres and IP velocities. It is shown that the spectral line shape for PBs and the angular dependence are modified with the increase of the target radius. The carried out analysis makes it possible to determine an optimum region of parametric variation, in which the use of PBs spectroscopy for investigation of the structure and physical properties of metal nanoparticles in a dielectric matrix is most promising.

8.3 Bremsstrahlung of Fast Electrons on Graphene

8.3.1 Cross-Section of Bremsstrahlung on Graphene

8.3.1.1 General Expression for the Cross-Section of the Process on an Ensemble of Atoms

The cross-section of a photoprocess on an ensemble of target atoms looks like (in case of a monatomic target) [14]:

$$d\sigma_{target} = \left| \sum_j \exp\left(i\,\mathbf{q}\,\mathbf{r}_j\right) \right|^2 d\sigma_{atom}, \tag{8.34}$$

where the sum is over all target atoms being in the volume of interaction, $d\sigma_{atom}$ is the differential cross-section of the process on one atom under consideration,

$$\mathbf{q} = \left(\mathbf{p}_f - \mathbf{p}_i\right)/\hbar + \mathbf{k}$$

is the wave vector transferred from an incident electron to the target, $\mathbf{p}_i$, $\mathbf{p}_f$ are the initial and finite electron momenta, $\mathbf{k}$ is the wave vector of a photon.

In the state of thermodynamic equilibrium the squared absolute value in the formula (8.34) should be properly averaged:

$$\left|\sum_j \exp\left(i\,\mathbf{q}\,\mathbf{r}_j\right)\right|^2 \to \left\langle \sum_{j,j'} \exp\left(i\,\mathbf{q}\,\left(\mathbf{r}_j - \mathbf{r}_{j'}\right)\right)\right\rangle.$$

8.3.1.2 Structure Factor of a Three-dimensional Crystal

The structure factor of a medium in a three-dimensional case (a three-dimensional single crystal, the angle brackets mean averaging over atom positions) [14]:

$$\left\langle \sum_{j,j'} \exp\left(i\,\mathbf{q}\,\left(\mathbf{r}_j - \mathbf{r}_{j'}\right)\right)\right\rangle = N\left(1 - \exp\left(-u^2\,q^2\right)\right) + N\,n_a\,(2\pi)^3 \sum_{\mathbf{g}} e^{-u^2\,g^2}\,|S(\mathbf{g})|^2\,\delta^{(3)}(\mathbf{q}-\mathbf{g}), \quad (8.35)$$

where $N = N_0\,N_{cell}$ is the full number of atoms in the volume of interaction, N_0 is the full number of cells in the volume of interaction, N_{cell} is the number of atoms in a cell, $\mathbf{g}$ is the wave vector of a reciprocal lattice, $n_a = N_{cell}/\Delta_{cell}$ is the volume concentration of atoms, Δ_{cell} is the volume of a unit cell.

In the formula (8.35) the value $S(\mathbf{q})$ is introduced – the *normalized* structure factor of a unit cell of a crystal on the wave vector $\mathbf{q}$, $S(\mathbf{q}=0) = 1$, $\delta^{(3)}(\mathbf{q}) = \delta(q_x)\,\delta\left(q_y\right)\,\delta(q_z)$ is the three-dimensional delta function of the wave vector transferred to the target.

It should be noted that in the book [14] the *nonnormalized* structure factor of a cell is used.

8.3.1.3 Structure Factor of a Two-dimensional Crystal

In going to a two-dimensional case (we assume that a two-dimensional single crystal lies in the $x\,y$ plane, the z coordinate is fixed: $z = z_0$; graphene), when:

$$\mathbf{q}\,\mathbf{r}_j = q_z\,z_0 + \mathbf{q}_{\|}\,\rho_j,$$

for the structure factor of the target by analogy with the three-dimensional case we have

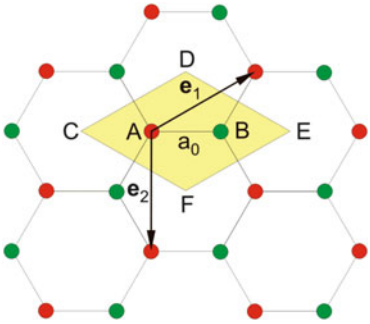

Fig. 8.12 The crystal structure of graphene. A unit cell (CDEF) and elementary translation vectors ($\mathbf{e}_1$, $\mathbf{e}_2$) are shown (The author Alexander Mayorov, InterNet)

$$\left\langle \sum_{j,j'} \exp\left(i\,\mathbf{q}_{\|}\left(\rho_j - \rho_{j'}\right)\right)\right\rangle = N\left(1 - \exp\left(-u^2\,q_{\|}^2\right)\right) + N\,n_s\,(2\pi)^2 \sum_{\mathbf{g}} e^{-u^2\,g^2}\,|S(\mathbf{g})|^2\,\delta^{(2)}\left(\mathbf{q}_{\|} - \mathbf{g}\right), \tag{8.36}$$

where ρ_j is the radius vector of an atom in the plane of the two-dimensional crystal, $\boldsymbol{\rho} = (x, y)$, $\delta^{(2)}\left(\mathbf{q}_{\|}\right) = \delta(q_x)\,\delta\left(q_y\right)$ is the two-dimensional delta function, n_s is the two-dimensional concentration of atoms, u is the root-mean-square deviation of atoms from the equilibrium position. The case $u = 0$ corresponds to going to a perfect crystal.

In Fig. 8.12 the crystal structure of graphene is presented.

The following values are introduced: $a = \sqrt{3}\,a_0 = 0.246$ nm is the lattice constant for graphene, $a_0 = 0.142$ nm is the distance between the nearest atoms (the distance between the atoms in a unit cell, graphene has *two atoms* in a unit cell).

8.3.1.4 Structure Factor of a Unit Cell of Graphene

We assume that an atom A (Fig. 8.12) is at the origin of coordinates, then

$$S(\mathbf{q}) = \frac{1}{2}[1 + \exp(i\,\mathbf{q}\,\mathbf{r}_B)]. \tag{8.37}$$

From Fig. 8.12 it follows that

$$\mathbf{r}_B = \frac{2}{3}\,\mathbf{e}_1 + \frac{1}{3}\,\mathbf{e}_2,$$

where $\mathbf{e}_1 = \left(\frac{\sqrt{3}\,a}{2}, -\frac{a}{2}\right)$ and $\mathbf{e}_1 = (0, a)$ are the basis vectors if the y-axis is directed straight down. Displacing a unit cell by these vectors, it is possible to reproduce the

whole crystal lattice of graphene. Then for the graphene reciprocal lattice vectors we have

$$\mathbf{g}_1 = \left(4\,\pi\Big/\sqrt{3}\,a, 0\right),\ \ \mathbf{g}_2 = \left(2\,\pi\Big/\sqrt{3}\,a, 2\,\pi/a\right), \tag{8.38}$$

so $\mathbf{e}_i\,\mathbf{g}_j = 2\,\pi\,\delta_{ij}$ according to the definition of the reciprocal lattice vector.

In the Cartesian coordinates ($y_B = 0$) it can be written:

$$\mathbf{g}\,\mathbf{r}_B = g_x\,x_B + g_y\,y_B = g_x\,x_B = g_x\,a\Big/\sqrt{3},$$

where the reciprocal lattice vector is:

$$\mathbf{g} = n_1\,\mathbf{g}_1 + n_2\,\mathbf{g}_2, \tag{8.39}$$

$n_{1,2}$ are the integers and

$$g_x = n_1\,g_{1x} + n_2\,g_{2x}.$$

Thus the scalar product included in determination of the structure factor of a unit cell of graphene (Eq. 8.37) is

$$\mathbf{g}\,\mathbf{r}_B = \frac{4\,\pi}{3}\,n_1 + \frac{2\,\pi}{3}\,n_2. \tag{8.40}$$

Accordingly, the structure factor of a unit cell of graphene is

$$S(\mathbf{g}) = \frac{1}{2}\left[1 + \exp\left(i\,(2\,n_1 + n_2)\,\frac{2\,\pi}{3}\right)\right]. \tag{8.41}$$

Hence for the squared absolute value of the structure factor of graphene we find

$$|S(\mathbf{g})|^2 = \frac{1}{2}\left[1 + \cos\left(\frac{2\,\pi}{3}\,(2\,n_1 + n_2)\right)\right]. \tag{8.42}$$

The magnitude of the graphene reciprocal lattice vector can be determined in view of the above expressions:

$$g(n_1,\,n_2) = \frac{4\,\pi}{\sqrt{3}\,a}\,\sqrt{n_1^2 + n_2^2 + n_1\,n_2}. \tag{8.43}$$

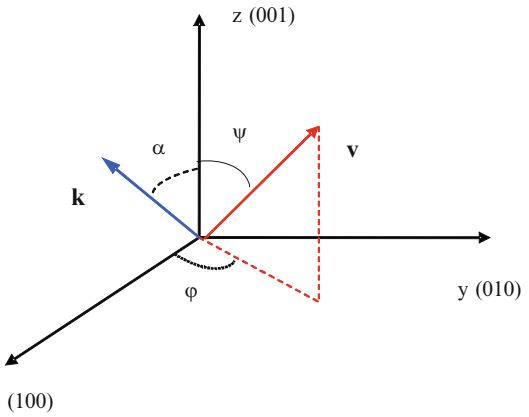

Fig. 8.13 The geometry of the process: α is the angle of photon emission with respect to the normal of the graphene plane, ψ is the polar angle of electron incoming with respect to the normal of the graphene plane, φ is the azimuth angle of electron incoming

The two-dimensional concentration of graphene atoms that is included in the structure factor of the two-dimensional crystal is

$$n_s = \frac{N_{cell}}{S_{cell}}.$$

The number of atoms in a unit cell of graphene is $N_{cell} = 2$, the area of a unit cell is $S_{cell} = \frac{\sqrt{3}\,a^2}{2}$, so

$$n_s = \frac{4}{\sqrt{3}\,a^2}. \tag{8.44}$$

Let us consider bremsstrahlung arising as a result of electron scattering by the two-dimensional plane of graphene. The geometry of the process is shown in Fig. 8.13.

8.3.2 *Cross-Section of Polarization Bremsstrahlung on a Carbon Atom*

The cross-section of polarization bremsstrahlung on an atom, differential with respect to the frequency and the solid angle of photon escape, is

$$\frac{d\sigma_a^{(PB)}}{d\omega\, d\Omega_{\mathbf{k}}} = \frac{e^2}{\hbar\,\omega}\,\frac{c}{\pi^2\,\mathrm{v}}\int \delta(\omega - \mathbf{k}\,\mathbf{v} + \mathbf{q}\,\mathbf{v})\,\frac{\left[\mathbf{s},\,\omega\,\mathbf{v}/c^2 - \mathbf{q}\right]^2}{\left(\mathbf{q}^2 - 2\,\mathbf{k}\,\mathbf{q}\right)^2}\left|\left(\frac{\omega}{c}\right)^2 \alpha(\omega,\,\mathbf{q})\right|^2 d\mathbf{q}, \tag{8.45}$$

where $\alpha(\omega,\,\mathbf{q})$ is the generalized dynamic polarizability of an atom, $\mathbf{s} = \mathbf{k}/|\mathbf{k}|$ is the unit vector in the direction of photon emission.

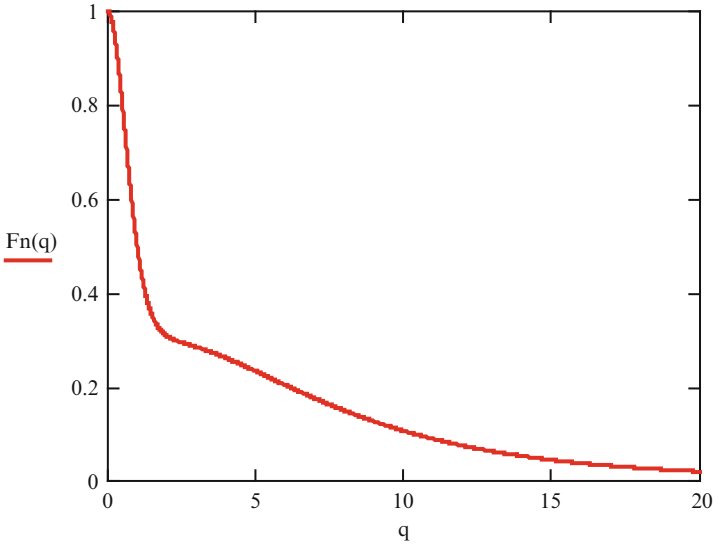

Fig. 8.14 The normalized form factor of a carbon atom, the X-axis is plotted in atomic units

In the multiplicative approximation the generalized dynamic polarizability of an atom is expressed in terms of the dipole polarizability and the atomic form factor:

$$\alpha(\omega, \mathbf{q}) = \alpha(\omega)\,\tilde{F}(q), \tag{8.46}$$

where $\tilde{F}(q)$ is the atomic form factor normalized by the condition $\tilde{F}(q = 0) = 1$.

To calculate the atomic form factor $F(q)$ that within the framework of the multiplicative approximation defines the dependence of the generalized polarizability of an atom on the value of a transferred momentum (of a wave vector), it is convenient to use the Slater wave functions of atomic orbitals. As shown in the work [15], the form factor calculated in such a way differs from its Hartree-Fock analog by no more than units of percents. Corresponding formulas look like:

$$\tilde{F}(q) = \frac{1}{Z}\sum_j N_j\, Q\left(q, \beta_j, \mu_j\right),\ Q(q, \beta, \mu) = \frac{\left[1 + (q/2\beta)^2\right]^{\mu}}{(\mu\, q/\beta)} \sin\left[2\,\mu\,\mathrm{atan}\left(\frac{q}{2\,\beta}\right)\right],$$

where N_j is the number of equivalent electrons in the j th atomic shell, β and μ are the Slater parameters of atomic shells.

The normalized form factor of a carbon atom calculated according to the above formulas is presented in Fig. 8.14 as a function of the magnitude of the transferred wave vector q. The nonmonotonicity of decrease of the form factor with growing value q is connected with the shell structure of an atom. Corresponding to high values of q is the contribution to $\tilde{F}(q)$ of the inner shell of a carbon atom with the principal quantum number $n = 1$. Corresponding to small values of q is the second (outer)

atomic shell. A bend of the dependence $\tilde{F}(q)$ at $q \approx 1$ corresponds to transition from one electron shell to another.

Since the dynamic polarizability of an atom is a complex value, the real and imaginary parts of which are related by the Kramers-Kronig relations, it is convenient to begin its calculation with the imaginary part. To obtain the frequency dependence of the imaginary part of the dipole polarizability, we proceed from its relation with the cross-section of radiation absorption $\sigma_{ph}(\omega)$ given by the optical theorem:

$$\mathrm{Im}(\alpha(\omega)) = \frac{c}{4\pi\omega}\,\sigma_{ph}(\omega). \tag{8.47}$$

In this book, to determine the spectral dependence of the photoabsorption cross-section $\sigma_{ph}(\omega)$, the data on the radiation absorption coefficient given at the Internet site of the Berkeley National Laboratory are used.

The real part of the atomic polarizability can be restored by the known imaginary part with the use of the Kramers-Kronig relation that for calculations is convenient to be presented as follows:

$$\mathrm{Re}(\alpha(\omega)) = \frac{2}{\pi}\int_0^\infty \frac{\omega\mathrm{Im}(\alpha(\omega)) - \omega'\mathrm{Im}(\alpha(\omega'))}{\omega^2 - \omega'^2}\,d\omega'. \tag{8.48}$$

This equation, due to the presence of the second summand in the numerator of the integrand, allows calculation of the principal-value integral appearing in the standard form of the Kramers-Kronig relations in terms of a punctured integral with a "puncture" eliminating the singularity of the integrand, which is convenient in practical calculations. At high frequencies the imaginary part of the polarizability decreases as $\omega^{-9/2}$, so the integral on the right side of the equation converges well at infinity.

The results of calculation of the dynamic polarizability of a carbon atom are presented in Fig. 8.15. Given for comparison in the same figure is the number of electrons in a carbon atom, tending to which in the high-frequency limit is the real part of the atomic polarizability normalized to the polarizability of a free electron with the opposite sign: $\alpha(\omega) \to \alpha(\omega)/\left(-e^2/m\,\omega^2\right)$.

From this figure it is seen that in the high-frequency limit the imaginary part of the polarizability tends to zero. The peculiarities on the curves of Fig. 8.15 correspond to potentials of ionization of electron subshells of a carbon atom.

8.3.3 Polarization Bremsstrahlung on Graphene

If the expression for the structure factor of graphene (Eq. 8.36) is substituted in the general formula for the cross-section of bremsstrahlung on a polyatomic target (Eq. 8.34), two terms will appear in the Bs cross-section that correspond to the incoherent (the first summand on the right side of Eq. 8.36) and coherent (the second summand on the right side of Eq. 8.36) parts of the structure factor.

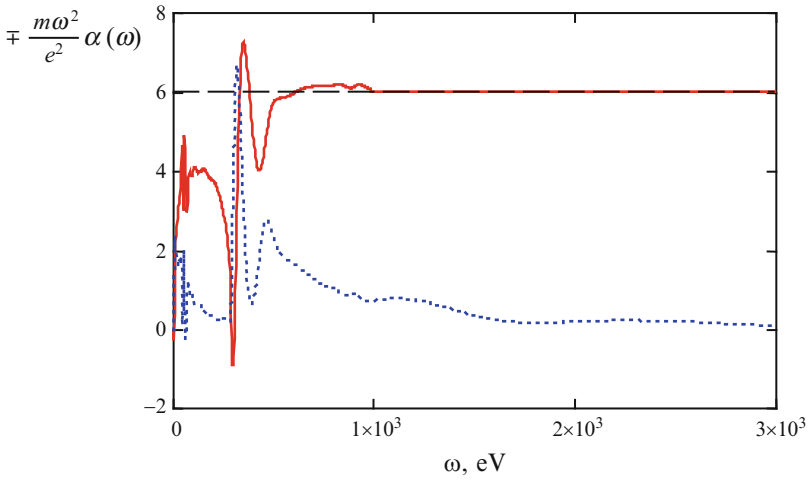

Fig. 8.15 The real (*solid curve*) and imaginary (*dotted curve*) parts of the dynamic polarizability of a carbon atom multiplied by the squared frequency, the Y-axis is plotted in dimensionless units, minus in the definition of the Y-axis relates to the real part and plus relates to the imaginary part of the polarizability

8.3.3.1 Incoherent PBs on Graphene

Substituting Eq. 8.36 in Eq. 8.34, we find that the cross-section of incoherent PBs on a target (in terms of one atom) is

$$\frac{1}{N}\frac{d\sigma^{(PB)}_{incoh}}{d\omega\, d\Omega_{\mathbf{k}}} = \frac{e^2}{\hbar\,\omega}\frac{c}{\pi^2\,\mathrm{v}}\int \delta(\omega - \mathbf{k}\,\mathbf{v} + \mathbf{q}\,\mathbf{v}) \times \left(1 - \exp\left(-u^2\,\mathbf{q}^2\right)\right)\frac{\left[\mathbf{s},\, \omega\,\mathbf{v}/c^2 - \mathbf{q}\right]^2}{\left(\mathbf{q}^2 - 2\,\mathbf{k}\,\mathbf{q}\right)^2}\left|\left(\frac{\omega}{c}\right)^2\alpha(\omega,\, q)\right|^2 d\mathbf{q}. \tag{8.49}$$

Integration on the right side of this equation with respect to the angles of the vector $\mathbf{q}$ in view of the presence of the delta function gives:

$$\frac{1}{N}\frac{d\sigma^{(PB)}_{incoh}}{d\omega\, d\Omega_{\mathbf{k}}} = \frac{2\,e^2}{\pi\,\mathrm{v}^2\,\mathrm{c}^3\,\hbar\omega}\int\limits_{q_{\min}}^{q_{\max}}\frac{dq}{q}\,I_{\varphi}(q,\,\mathrm{v},\,\omega,\,\theta)\left(1 - e^{-u^2\,q^2}\right)\left|\omega^2\,\alpha(\omega,\,q)\right|^2, \tag{8.50}$$

where

$$q_{\min}(\omega,\mathrm{v},\theta) = \frac{\omega}{\mathrm{v}}\left(1 - \frac{\mathrm{v}}{c}\cos\theta\right),\; q_{\max} = 2\mu\;\mathrm{v}/\hbar,$$

μ is the reduced mass of an electron and a target atom, $\theta = angle(\mathbf{k}, \mathbf{v})$ is the radiation angle,

$$I_\varphi(q, \mathrm{v}, \omega, \theta) = \frac{q^3\,\mathrm{v}}{2\,\pi}\int d\Omega_{\mathbf{q}}\,\delta(\omega - \mathbf{kv} + \mathbf{qv})\,\frac{\left[\mathbf{s}, \omega\,\mathbf{v}/c^2 - \mathbf{q}\right]^2}{\left(\mathbf{q}^2 - 2\,\mathbf{k}\,\mathbf{q}\right)^2} \tag{8.51}$$

is the dimensionless kinematic integral calculated in the explicit form in [5], $d\Omega_{\mathbf{q}}$ is the element of the solid angle around the vector $\mathbf{q}$. In the nonrelativistic limit $\mathrm{v}<<c$ the kinematic integral looks like

$$I_\varphi(q, \mathrm{v}, \omega, \theta) \cong \frac{1 + \cos^2\theta}{2} + \left(\frac{\omega}{q\,\mathrm{v}}\right)^2\,\frac{1 - 3\cos^2\theta}{2}. \tag{8.52}$$

In the general case the kinematic integral can be represented as a function of three variables $I_\varphi(q, \mathrm{v}, \omega, \theta) = \tilde{I}_\varphi(x = q\,c/\omega, \beta = \mathrm{v}/\mathrm{c}, \theta)$, where

$$\tilde{I}_\varphi(x, \beta, \theta) = \frac{x^2 f_1(x, \beta, \theta)}{\Delta^{3/2}(x, \beta, \theta)} + \frac{x^2}{4}\left[\frac{f_2(x, \beta, \theta)}{\Delta^{1/2}(x, \beta, \theta)} - 1\right], \tag{8.53}$$

$$f_1 = \left(x^2 + 2\,\tilde{x}\,\cos\theta\right)\left[\left(x^2 - \tilde{x}^2\right)\cos^2\theta + (\tilde{x} - \beta)^2\sin^2\theta\right] + 4\,\sin^2\theta\,\cos\theta\,(\tilde{x} - \beta)\left(x^2 - \tilde{x}^2\right),$$

$$f_2 = x^2 + 2\,\tilde{x}\,\cos\theta,\ \tilde{x} = q_{\min}\frac{c}{\omega} = \beta^{-1} - \cos\theta,$$

$$\Delta = \left(x^2 - 2\left(1 - \frac{\cos\theta}{\beta}\right)\right)^2 + 4\frac{1 - \beta^2}{\beta^2}\,\sin^2\theta.$$

In the relativistic limit ($\beta \to 1$) the function $\tilde{I}_\varphi(x, \beta, \theta)$ has a sharp maximum in fulfilment of the equation $x_{\max} = \sqrt{2\,(1 - \cos\theta/\beta)} \approx 2\,\sin(\theta/2)$, and the sharpness of the maximum increases for wide radiation angles $\theta \to \pi$. This maximum corresponds to exit of a photon "to the mass shell" in case of propagation of an electromagnetic field in a medium.

8.3.3.2 Coherent PBs on Graphene

The cross-section of coherent PBs on a two-dimensional periodic structure, which is graphene, (in terms of one atom) is

$$\frac{1}{N}\frac{d\sigma_{coh}^{(PB)}}{d\omega\, d\Omega_{\mathbf{k}}} = \frac{e^2}{\hbar\,\omega}\frac{c}{\pi^2\,\mathrm{v}}\left(\frac{\omega}{c}\right)^4 n_s\,(2\,\pi)^2\times$$
$$\sum_{\mathbf{g}} e^{-u^2\,(\mathbf{g}+\mathbf{q}_\perp)^2}\,|S(\mathbf{g})|^2\int\delta(\omega-\mathbf{k}\,\mathbf{v}+\mathbf{g}\,\mathbf{v}+q_z\mathrm{v}_z)$$
$$\times\frac{\left[\mathbf{s},\,\omega\,\mathbf{v}/c^2-(\mathbf{g}+\mathbf{q}_\perp)\right]^2}{\left((\mathbf{g}+\mathbf{q}_\perp)^2-2\,\mathbf{k}\,(\mathbf{g}+\mathbf{q}_\perp)\right)^2}\,|\alpha(\omega,\,\mathbf{g}+\mathbf{q}_\perp)|^2 dq_z. \tag{8.54}$$

In derivation of this expression it was taken into account that integration with respect to the two-dimensional delta function $\delta^{(2)}\left(\mathbf{q}_\parallel-\mathbf{g}\right)$ gives:

$$\mathbf{q}_\parallel=\mathbf{g}, \tag{8.55}$$

and there remains integration with respect to the component of the wave vector dq_z transferred to the target, this component being normal to the graphene plane, the said integration is also "removed" due to the presence of the delta function $\delta(\omega-\mathbf{k}\,\mathbf{v}+\mathbf{g}\,\mathbf{v}+q_z\mathrm{v}_z)$ under the sign of integration. As a result, we find a fixed value for the normal (to the graphene plane) component of the wave vector transferred to the target as a function of the problem parameters:

$$q_z=-g\,tg\psi+\frac{\omega-\mathbf{k}\,\mathbf{v}}{\mathrm{v}\cos\psi}. \tag{8.56}$$

This value should be substituted in the expression for the coherent PBs cross-section ($|\mathbf{q}_\perp|=q_z$). Taking into account the fact that $(\mathbf{q}_\perp\,\mathbf{g})=0$ and in view of the relation (8.46), we obtain for the differential spectral-angular cross-section of coherent PBs on graphene the following expression:

$$\frac{1}{N}\frac{d\sigma_{coh}^{(PB)}}{d\omega\, d\Omega_{\mathbf{k}}}=\frac{4\,n_s}{\cos\psi}\left(\frac{e^2}{\hbar\,\omega}\right)\frac{\omega^4\,|\alpha(\omega)|^2}{c^3\,\mathrm{v}^2}$$
$$\times\sum_{\mathbf{g}} e^{-u^2\,\left(g^2+q_z^2\right)}\,|S(\mathbf{g})|^2\left|\tilde{F}\left(\sqrt{g^2+q_z^2}\right)\right|^2 P(\mathbf{g},\,\mathbf{k},\,\mathbf{q}_\perp), \tag{8.57}$$

where

$$P(\mathbf{g},\,\mathbf{k},\,q_z)$$
$$=\frac{\left(\frac{\omega\,\mathrm{v}}{c^2}\right)^2+g^2+q_z^2-2\,\frac{\omega\,\mathrm{v}}{c^2}(g\,\sin\psi+q_z\,\cos\psi)-\left[\frac{\omega\,\mathrm{v}}{c^2}\cos\theta-g\,\sin\alpha-q_z\,\cos\alpha\right]^2}{\left(g^2+q_z^2-2\,\frac{\omega}{c}\,(g\,\sin\alpha+q_z\,\cos\alpha)\right)^2}, \tag{8.58}$$

$$|S(\mathbf{g})|^2 = \cos^2\Big(\frac{\pi}{3}(2\,n_1 + n_2)\Big),\ |\mathbf{g}| = g(n_1,\,n_2) = \frac{4\,\pi}{\sqrt{3}\,a}\,\sqrt{n_1^2 + n_2^2 + n_1\,n_2}$$

$$\cos\theta = \cos\alpha\,\cos\psi + \cos\varphi\,\sin\alpha\,\sin\psi,\ n_s = \frac{4}{\sqrt{3}\,a^2},$$

and

$$q_z = -g\,tg\psi + \omega\frac{1 - (\mathrm{v}/c)\,\cos\theta}{\mathrm{v}\cos\psi}.$$

Summation over the reciprocal lattice vectors $\mathbf{g}$ implies summation over the integers $n_{1,2}$ defining the magnitude of $\mathbf{g}$.

It should be noted that in contrast to coherent PBs in a three-dimensional single crystal, when the radiated frequency is fixed by the condition

$$\omega_{\max}^{(3)} = -\frac{\mathbf{g}\,\mathbf{v}}{1 - \beta\,\cos\theta}, \tag{8.59}$$

hence we find for a cubic crystal ($n_{1,2,3}$ are the integers):

$$\omega_{\max}^{(3)} = -\frac{g\,\mathrm{v}\,(n_1\,\sin\psi\,\cos\varphi + n_2\,\sin\psi\,\sin\varphi + n_3\,\cos\psi\,)}{1 - \beta\,\cos\theta}, \tag{8.60}$$

the frequency of coherent PBs in a two-dimensional single crystal is not a fixed value. Nevertheless, in the two-dimensional case with fulfilment of certain conditions (see below) the PBs spectrum has sharp maxima. The frequencies of these maxima are defined by the zeros of the denominator $P(\mathbf{g},\,\mathbf{k},\,q_z)$ in the expression for the coherent PBs cross-section (Eq. 8.57).

For the denominator $P(\mathbf{g},\,\mathbf{k},\,q_z)$, taking into account the explicit form of q_z, we find:

$$\mathrm{Den}(\omega,\,\alpha,\psi,\beta,\theta) = \frac{g^4}{\cos^4\psi}\Big\{\Big(\frac{\omega}{g\,\mathrm{v}}\Big)^2\,\delta\,[\delta - 2\,\beta\,\cos\alpha\,\cos\psi] + 2\,\beta\,\frac{\omega}{g\,\mathrm{v}}\,\cos\psi\,[\cos\alpha\,\sin\psi - \sin\alpha - \frac{\delta}{\beta}\,tg\psi] + 1\Big\}^2, \tag{8.61}$$

where the contracted notations $\delta = 1 - \beta\,\cos\theta$, $\beta = \mathrm{v}/c$ are introduced, and the cosine of the radiation angle is $\cos\theta = \cos\alpha\,\cos\psi + \cos\varphi\,\sin\alpha\,\sin\psi$.

For the zero angle of electron incoming into the graphene plane ($\psi = 0$) the expression for the denominator is simplified to the form:

$$\begin{aligned}&\mathrm{Den}(\omega,\ \alpha, \psi = 0, \beta, \theta = \alpha)\\&= g^4 \left\{ \left(\frac{\omega}{g\,\mathrm{v}} \right)^2 (1 - \beta\,\cos\alpha)\,(1 - 3\,\beta\,\cos\alpha) - 2\,\beta\,\frac{\omega}{g\,\mathrm{v}}\,\sin\alpha + 1 \right\}^2 .\end{aligned} \tag{8.62}$$

The resonance condition for the coherent PBs cross-section in the general case looks like

$$\mathrm{Den}(\omega,\ \alpha, \psi, \beta, \theta) = 0. \tag{8.63}$$

If this equation is solved with respect to the radiation frequency, the following expression for the frequency of a spectral maximum in coherent PBs on graphene will be obtained:

$$\omega_{\max} = g\,\mathrm{v}\,F_\omega(\alpha, \psi, \theta, \beta). \tag{8.64}$$

Here the dimensionless function is introduced:

$$\begin{aligned}&F_\omega(\alpha, \psi, \theta, \beta)\\&= \frac{\cos\psi\,(\beta\,\sin\alpha + \delta\,tg\psi - \beta\,\sin\psi\,\cos\alpha) + \mathrm{sign}(\delta - 2\,\beta\cos\alpha\,\cos\psi)\,\sqrt{D}}{\delta(\delta - 2\,\beta\cos\alpha\,\cos\psi)},\end{aligned} \tag{8.65}$$

where $\delta = 1 - \beta\,\cos\theta, \beta = \mathrm{v}/c, D = \cos^2\psi\,(\beta\,\sin\alpha + tg\psi\,\delta - \beta\,\sin\psi\,\cos\alpha)^2 - \delta\,(\delta - 2\,\beta\cos\alpha\,\cos\psi)$ and

$$\mathrm{sign}(x) = \begin{cases} 1 & \text{for } x>0 \\ 0 & \text{for } x = 0\,. \\ -1 & \text{for } x<0 \end{cases}$$

In case of the zero angle of electron incoming into a two-dimensional single crystal ($\psi = 0$), we have the following expression for the function determining the dependence of the resonance frequency of radiation on the electron velocity and the angle of photon emission:

$$\begin{aligned}&F_\omega(\psi = 0)\\&= \frac{\beta\,\sin\alpha + \mathrm{sign}(1 - 3\,\beta\,\cos\alpha)\,\sqrt{(\beta\,\sin\alpha)^2 - (1 - \beta\,\cos\alpha)\,(1 - 3\beta\,\cos\alpha)}}{(1 - \beta\,\cos\alpha)\,(1 - 3\beta\,\cos\alpha)}.\end{aligned} \tag{8.66}$$

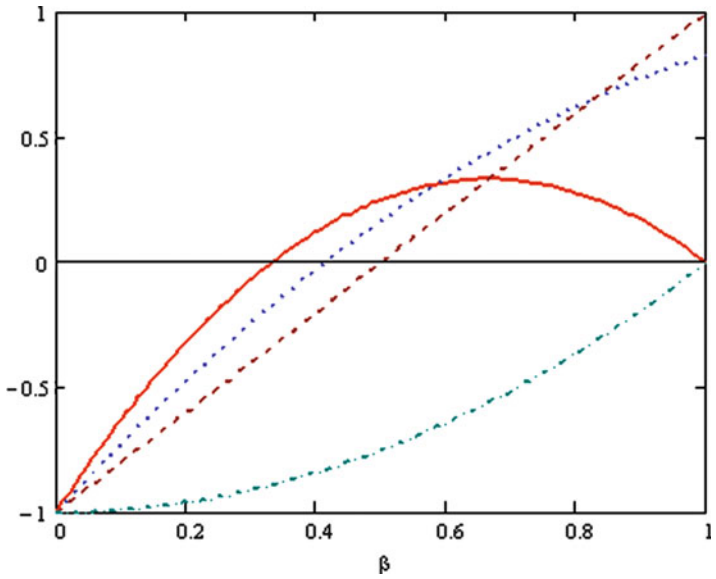

Fig. 8.16 The dependence of the discriminant (8.67) defining the resonance frequency of PBs for the zero angle of electron incoming $\psi = 0$ on the electron velocity ($.\gamma \propto r_s^3.$) for different radiation angles α: *solid line* – $\alpha = 0$, *dotted line* – $\alpha = \pi/4$, *dashed line* – $\alpha = \pi/3$, *dotted-dashed line* $\alpha = \pi/2$

For the positiveness of the discriminant in this expression

$$D\omega(\alpha, \beta) = (\beta \sin\alpha)^2 - (1 - \beta\cos\alpha)(1 - 3\beta\cos\alpha), \tag{8.67}$$

that is, for existence of a resonance frequency of coherent PBs the fulfilment of the condition is required:

$$\frac{1}{2\cos\alpha - 1} \geq \beta \geq \frac{1}{2\cos\alpha + 1}. \tag{8.68}$$

Following hence is the necessary condition of the presence of a resonance $2\cos\alpha + 1 > 1$, that is, $\alpha < \pi/2$ – radiation should go to the top hemisphere $z > 0$ (see Fig. 8.13).

The dependence of the discriminant (8.67) on the electron velocity for different radiation angles for the zero angle of electron incoming is presented in Fig. 8.16.

From this figure it is seen that with increasing radiation angle the range of electron velocity values decreases, in which the discriminant is positive, that is, there is a resonance in the cross-section of coherent PBs on graphene. For the angle $\alpha = \pi/2$ this range comes to the point $v = c$.

If the equation $1 - 3\beta\cos\alpha = 0$ is satisfied, then, as follows from the formulas (8.64) and (8.66), the resonance frequency of coherent PBs becomes infinite, that is, a resonance is absent. So the equation

$$\beta = \frac{1}{3\,\cos\alpha}\left(> \frac{1}{2\,\cos\alpha + 1}\ \text{for}\ \alpha < \pi/2\right) \tag{8.69}$$

means the absence of a resonance. In turn, it is possible if $\alpha < \arccos(1/3)$.

Thus the analysis of coherent PBs in case of normal electron incoming has shown in particular that for small enough radiation angles $\alpha < \arccos(1/3)$ with the condition $3\,\cos\alpha = c/\mathrm{v}$ satisfied spectral resonances in radiation are absent since the resonance frequency becomes infinite.

It should be noted that if the discriminant (8.67) is negative, but is close to zero, the cross-section of coherent PBs on graphene also has maxima, but not so sharp as in case of the positive discriminant.

The total cross-section of electron PBs on graphene in terms of one atom is equal to the sum of the incoherent and coherent parts:

$$\frac{1}{N}\,\frac{d\sigma^{(PB)}}{d\omega\,d\Omega_{\mathbf{k}}} = \frac{1}{N}\,\frac{d\sigma^{(PB)}_{incoh}}{d\omega\,d\Omega_{\mathbf{k}}} + \frac{1}{N}\,\frac{d\sigma^{(PB)}_{coh}}{d\omega\,d\Omega_{\mathbf{k}}}. \tag{8.70}$$

8.3.4 Static Bremsstrahlung on Graphene

The expression for the cross-section of static bremsstrahlung of a relativistic charged particle on an atom (without its excitation) in the first Born approximation looks like [16]:

$$\frac{d\sigma^{OB}_{el}}{d\omega\ d\Omega_{\mathbf{k}}} = \frac{1}{4\pi^2\,\omega}\,\frac{e_p^2}{\hbar\,c}\,Z^2\,r_e^2\left(\frac{p_f}{p_i}\right)\left(\frac{m}{m_p}\right)^2\int d\Omega_{\mathbf{p}_f}\left[1-\tilde{F}_a(q)\right]^2 J\left(\Omega_{\mathbf{p}_f}\right), \tag{8.71}$$

where m_p is the mass of an incident particle and $J\left(\Omega_{\mathbf{p}_f}\right)$ is the dimensionless function determined by the equations:

$$\begin{aligned} J\left(\Omega_{\mathbf{p}_f}\right) = \frac{m_p^2}{(\hbar\,q)^4}\Bigg\{ & \left(\frac{p_f}{\kappa_f}\right)^2\left(4\,\varepsilon_i^2-(\hbar qc)^2\right)\,\sin^2\theta' \\ & +\left(\frac{p_i}{\kappa_i}\right)^2\left(4\,\varepsilon_f^2-(\hbar qc)^2\right)\,\sin^2\theta+\frac{2(\hbar\omega)^2}{\kappa_i\,\kappa_f}\left(p_i^2\sin^2\theta+p_f^2\sin^2\theta'\right) \\ & -\frac{2p_ip_f}{\kappa_i\,\kappa_f}\left[2\left(\varepsilon_i^2+\varepsilon_f^2\right)-(\hbar qc)^2\right]\sin\theta\sin\theta'\cos\varphi\Bigg\}, \end{aligned}$$

$$\kappa_i = \varepsilon_i/c - c(\mathbf{kp}_i)/\omega,\ \kappa_f = \varepsilon_f/c - c\left(\mathbf{kp}_f\right)/\omega,$$

$$\hbar q = \sqrt{(\hbar k)^2 + p_i^2 + p_f^2 - 2p_i\hbar k\cos\theta + 2p_f\hbar k\cos\theta' - 2p_i p_f\left(\cos\theta\cos\theta' + \sin\theta\sin\theta'\cos\varphi\right)},$$

θ' is the angle between the vectors $\mathbf{p}_f$ and $\mathbf{k}$, φ is the angle between the planes $\mathbf{p}_i\,\mathbf{k}$ and $\mathbf{p}_f\,\mathbf{k}$, $r_e = \frac{e^2}{mc^2}$.

The approximate formula for the differential cross-section of SBs on an atom looks like:

$$\frac{d\sigma_{el}^{OB}}{d\omega\; d\Omega_{\mathbf{k}}} \approx \frac{1}{\pi}\,\frac{Z^2\,e^6\,(1+\cos^2\theta)\left(1-\left(\frac{\mathrm{v}}{c}\right)^2\right)}{m^2\,\hbar\,\omega\,\mathrm{v}^2\,c^3\left(1-\frac{\mathrm{v}}{c}\cos\theta\right)^2}\int\limits_{q_{\min}}^{q_{\max}}\frac{\left(1-\tilde{F}(q)\right)^2}{q}dq, \tag{8.72}$$

where

$$q_{\min}(\omega,\mathrm{v},\theta) = \frac{\omega}{\mathrm{v}}\left(1-\frac{\mathrm{v}}{c}\cos\theta\right),\; q_{\max} = 2\mu\;\mathrm{v}/\hbar,$$

μ is the reduced mass of an electron and a target atom, $\theta = angle(\mathbf{k},\,\mathbf{v})$ is the radiation angle.

The expression (8.72) has a characteristic error of 10–30 % in comparison with the formula (8.71). In derivation of Eq. 8.72 the approximate equation for electron energy change during bremsstrahlung was used:

$$\varepsilon_f - \varepsilon_i \approx \hbar(\mathbf{q}-\mathbf{k})\,\mathbf{v}.$$

In the nonrelativistic limit $\mathrm{v}<<c$ from the expression (8.72) the equation follows:

$$\frac{d\sigma_{el}^{OB}}{d\omega\; d\Omega_{\mathbf{k}}} \approx \frac{1}{\pi}\,\frac{Z^2\,e^6\,(1+\cos^2\theta)}{m^2\,\hbar\,\omega\,\mathrm{v}^2\,c^3}\int\limits_{q_{\min}}^{q_{\max}}\frac{\left(1-\tilde{F}(q)\right)^2}{q}dq. \tag{8.73}$$

For the incoherent part of the cross-section of SBs on graphene (in terms of one atom) we have:

$$\frac{1}{N}\frac{d\sigma_{incoh}^{OB}}{d\omega\; d\Omega_{\mathbf{k}}} \approx \frac{1}{\pi}\,\frac{Z^2\,e^6\,(1+\cos^2\theta)\left(1-\left(\frac{\mathrm{v}}{c}\right)^2\right)}{m^2\hbar\omega\,\mathrm{v}^2\,c^3\left(1-\frac{\mathrm{v}}{c}\cos\theta\right)^2}\int\limits_{q_{\min}}^{q_{\max}}\frac{\left(1-\tilde{F}(q)\right)^2}{q}\left(1-\exp\left(-u^2\,q^2\right)\right)dq. \tag{8.74}$$

Given in Figs. 8.17 and 8.18 is the comparison of the spectral cross-sections of PBs and SBs on a carbon atom and incoherent PBs and SBs on graphene for an electron velocity of 100 a.u. (this velocity corresponds to an incident electron energy of 240 keV).

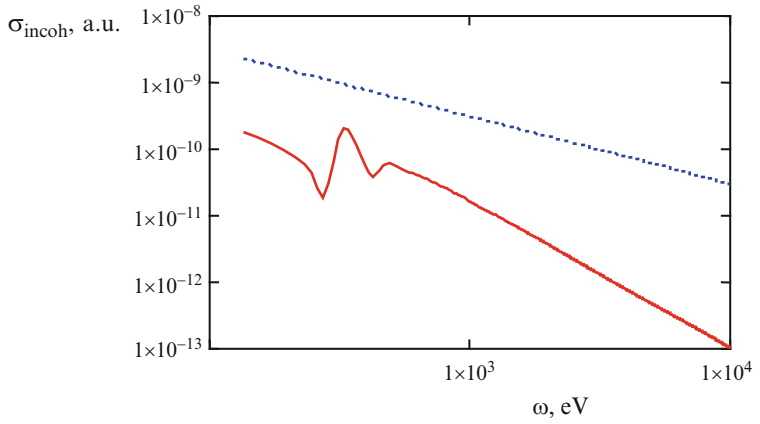

Fig. 8.17 The comparison of the spectral cross-sections of PBs (*solid curve*) and SBs (*dotted curve*) of an electron with a velocity of 100 a.u. scattered by a carbon atom, the radiation angle is $\theta = 30^\circ$, the abscissa is plotted in electron-volts, the ordinate is plotted in atomic units

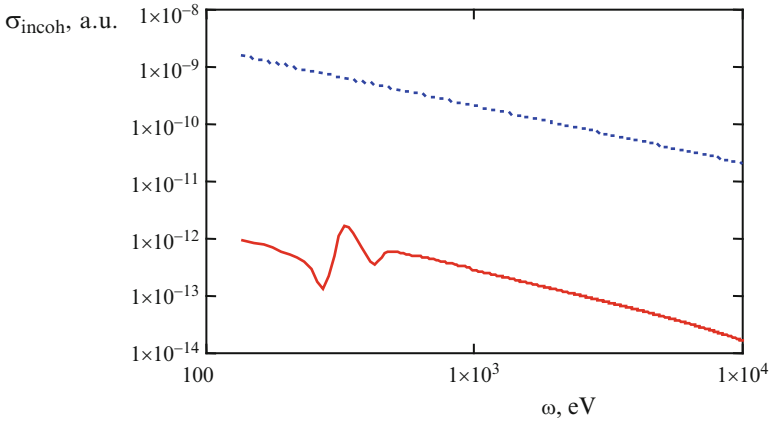

Fig. 8.18 The comparison of the spectral cross-sections of incoherent PBs (*solid curve*) and SBs (*dotted curve*) of an electron scattered by graphene (in terms of one atom), $v = 100$ a.u., the radiation angle is $\theta = 30^\circ$

From Fig. 8.17 it is seen that in case of a carbon atom the PBs cross-section at the maximum of the frequency dependence is about an order of magnitude less than the SBs cross-section. This circumstance is explained by relatively low dynamic polarizability of a carbon atom that defines the value of the PBs cross-section. With growing electron velocity the relative contribution of PBs will increase since the role of high impact parameters will increase.

The difference of incoherent channels of PBs and SBs on graphene is even more (Fig. 8.18) and is about two and a half orders of magnitude at the maximum of the spectral dependence of PBs. The latter circumstance is connected with the fact that the polarization channel is formed at long distances from a target, the contribution

of these distances to incoherent radiation is suppressed by the multiplier $1 - \exp(-u^2\, q^2)$ that is small for $q < 1/u$ (low impact parameters).

8.3.4.1 Coherent SBs on Graphene

For calculation of the coherent part of SBs on graphene it is necessary to express the cross-section of the process on an atom in terms of the integral with respect to the transferred wave vector **q**:

$$\frac{d\sigma_a^{OB}}{d\omega\; d\Omega_{\mathbf{k}}} \approx \frac{1}{2\,\pi^2}\,\frac{Z^2\, e^6\,(1+\cos^2\theta)\left(1-\left(\frac{\mathrm{v}}{c}\right)^2\right)}{\hbar\,\omega\, m^2\,\mathrm{v}\, c^3\left(1-\frac{\mathrm{v}}{c}\cos\theta\right)^2}\int\frac{\left(1-\tilde{F}(q)\right)^2}{q^2}\,\delta(\omega-\mathbf{k}\,\mathbf{v}+\mathbf{q}\,\mathbf{v})\,d\mathbf{q}. \tag{8.75}$$

Then the expression for the differential cross-section of coherent SBs on graphene (in terms of one atom) looks like:

$$\frac{1}{N}\,\frac{d\sigma_{coh}^{(OB)}}{d\omega\, d\Omega_{\mathbf{k}}} = \frac{Z^2\, e^6\,(1+\cos^2\theta)\left(1-\left(\frac{\mathrm{v}}{c}\right)^2\right)}{\hbar\,\omega\, m^2\,\mathrm{v}\, c^3\left(1-\frac{\mathrm{v}}{c}\cos\theta\right)^2}\, n_s \sum_{\mathbf{g}} e^{-u^2\,(\mathbf{g}+\mathbf{q}_\perp)^2}\,|S(\mathbf{g})|^2$$
$$\times\int\delta(\omega-\mathbf{k}\,\mathbf{v}+\mathbf{g}\,\mathbf{v}+q_z\mathrm{v}_z)\;\frac{\left[1-\tilde{F}(|\mathbf{g}+\mathbf{q}_\perp|)\right]^2}{(\mathbf{g}+\mathbf{q}_\perp)^2}\,dq_z. \tag{8.76}$$

The calculation of the integral on the right side of this equation in view of the delta function gives

$$\frac{1}{N}\,\frac{d\sigma_{coh}^{(OB)}}{d\omega\, d\Omega_{\mathbf{k}}} = frac2\, n_s \cos\psi\,\frac{Z^2\, e^6\,(1+\cos^2\theta)\left(1-\left(\frac{\mathrm{v}}{c}\right)^2\right)}{\hbar\,\omega\, m^2\,\mathrm{v}^2\, c^3\left(1-\frac{\mathrm{v}}{c}\cos\theta\right)^2}$$
$$\times\sum_{\mathbf{g}} e^{-u^2\left(g^2+q_z^2\right)}\,|S(\mathbf{g})|^2\,\frac{\left[1-\tilde{F}\left(\sqrt{g^2+q_z^2}\right)\right]^2}{g^2+q_z^2}, \tag{8.77}$$

where

$$q_z = -g\, tg\psi + \omega\frac{1-(\mathrm{v}/c)\,\cos\theta}{\mathrm{v}\cos\psi},\ \cos\theta = \cos\alpha\cos\psi + \cos\varphi\sin\alpha\sin\psi,$$

$$g(n_1,\, n_2) = \frac{4\,\pi}{\sqrt{3}\,a}\,\sqrt{n_1^2+n_2^2+n_1\, n_2}.$$

In view of the last equation summation over the reciprocal lattice vectors **g** in the formula (8.77) comes to summation over the set of the integers $(n_1,\, n_2)$.

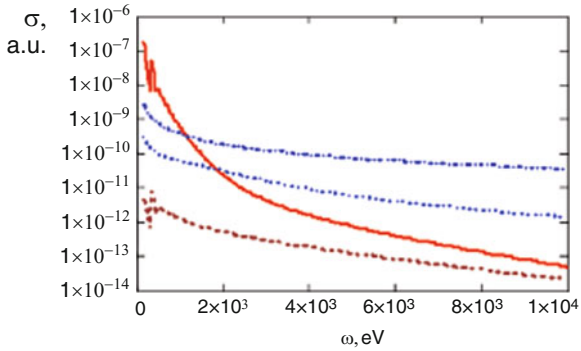

Fig. 8.19 The comparison of the cross-sections (in terms of one atom) of coherent and incoherent PBs and SBs of an electron on graphene for an electron energy of 30 keV ($v = 45$ a.u.), $\psi = 0$ and a radiation angle of 30°: *solid curve* – coherent PBs, *dotted curve* – coherent SBs, *dashed curve* – incoherent PBs, *dash-and-dot curve* – incoherent SBs

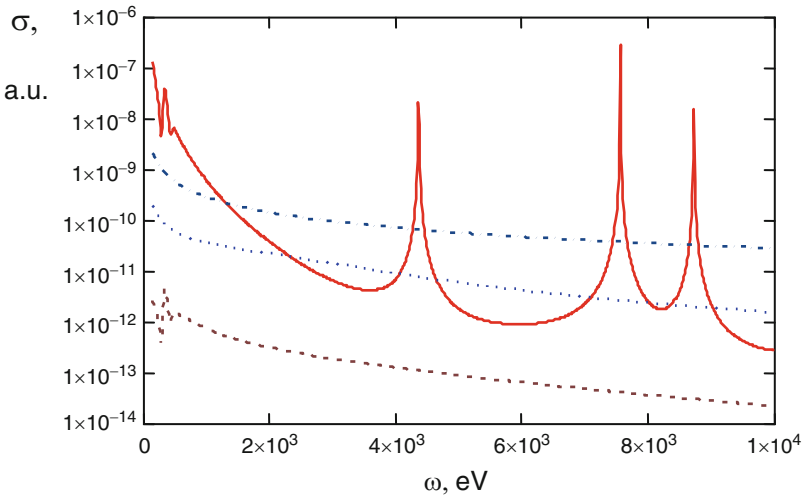

Fig. 8.20 The same as in Fig. 8.19 for an electron energy of 58 keV ($v = 60$ a.u.)

8.3.5 *Comparative Analysis of Contributions of Different Bremsstrahlung Channels in Electron Scattering on Graphene*

Let us calculate the contribution of different Bs channels in electron scattering on graphene with the use of expressions obtained in the previous section. The results of calculations are given in Figs. 8.19, 8.20, 8.21 and 8.22.

From Fig. 8.19 it follows that in case of a relatively low electron velocity of 45 a.u., which corresponds to the energy of 30 keV (at a specified radiation angle), spectral

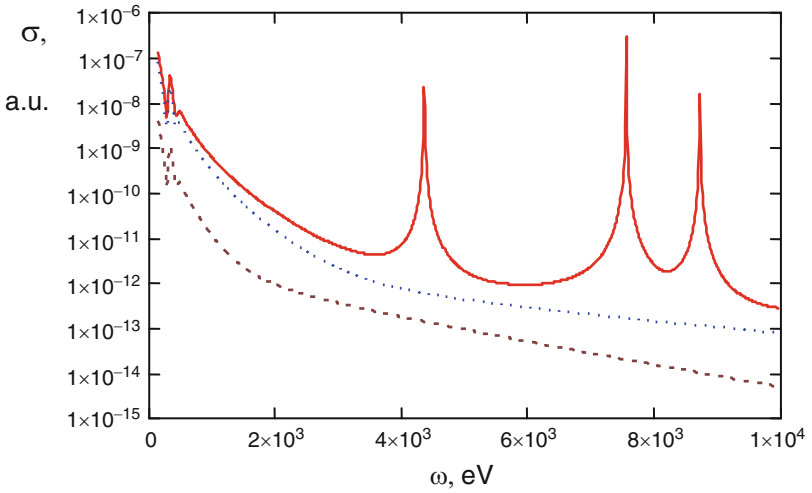

Fig. 8.21 The cross-section of coherent PBs of an electron on graphene for an electron energy of 58 keV (v = 60 a.u.), $\psi = 0$ and different radiation angles: *solid curve* – 30°, *dotted curve* – 60°, *dashed curve* – 120°

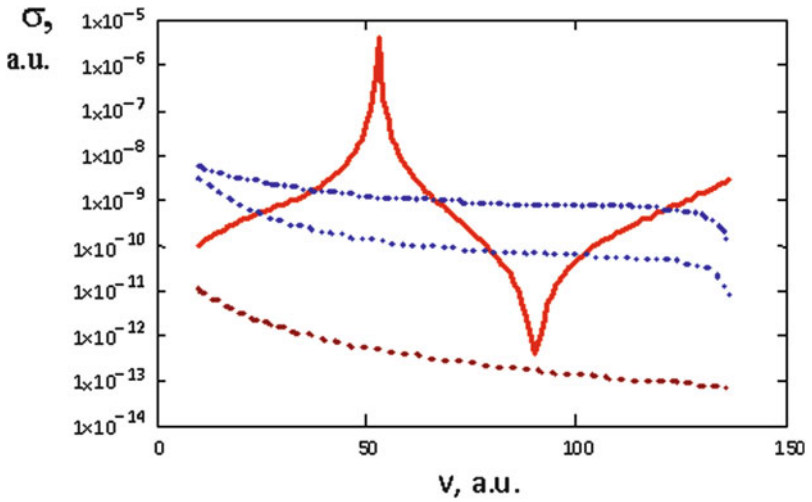

Fig. 8.22 The velocity dependences of coherent and incoherent PBs on graphene for the normal incidence of an electron, a photon energy of 272 eV, and a radiation angle of 30°: *solid curve* – coherent PBs, *dotted curve* – coherent SBs, *dashed curve* – incoherent PBs, *dash-and-dot curve* – incoherent SBs

resonances in the spectral range under consideration in the coherent PBs cross-section are absent. In this case coherent PBs prevails in the low-frequency region of the spectrum $\hbar\omega < 1 < 1$ keV, in the rest of the spectrum incoherent SBs prevails.

With growing electron velocity maxima appear in the coherent PBs cross-section at frequencies determined by the formulas (8.64) and (8.65) as seen from Fig. 8.20. Now near resonance frequencies a prevailing radiation channel is coherent PBs. With further increase of electron velocity the relative contribution of coherent PBs grows: it becomes comparable with incoherent SBs even far from resonances.

Given in Fig. 8.21 is the comparison of spectra of coherent PBs on graphene for a fixed electron velocity and different radiation angles.

It is seen that with growing radiation angle the maxima of the cross-section of coherent PBs in the spectral range under consideration disappear, and the value of the cross-section in a wide spectral range decreases.

The dependences of the cross-sections of different Bs channels on the electron velocity are presented in Fig. 8.22. From this figure it is seen that coherent PBs on graphene has sharp maximum and minimum. The velocity dependence of other Bs channels is monotonic. Deep minima in the cross-section of coherent PBs on graphene are caused by zeros of the function $P(\mathbf{g}, \mathbf{k}, q_z)$ (see the formula (8.58)) included in the expression for the cross-section (Eq. 8.57).

Thus the carried out analysis shows that the main contribution to bremsstrahlung of an electron on graphene is made by coherent polarization Bs and incoherent static Bs. It is found that the spectrum of coherent PBs of an electron on graphene for high enough velocities and small radiation angles contains sharp maxima corresponding to the vanishing denominator in the expression for the process cross-section. The spectral maxima in the cross-section of coherent PBs in a certain region of parametric variation take place in the angular and velocity dependences of the cross-section.

References

1. Lyalin, A.G., Solov'yov, A.V.: Polarization bremsstrahlung from atomic clusters. Rad. Phys. Chem. **75**, 1358 (2006)
2. Astapenko, V.A.: Bremsstrahlung of fast charged particles on clusters in a wide spectral range. JETP **101**, 3 (2005)
3. Astapenko, V.A., Buimistrov, V.M., Krotov, Y.A.: Bremsstrahlung accompanied by excitation and ionization of the scattering atoms. JETP **66**, 464 (1987)
4. Connerade, J.P., Solov'yov, A.V.: Giant resonances in photon emission spectra of metal clusters. J. Phys. B **29**, 3529 (1996)
5. Astapenko, V.A.: Polarization bremsstrahlung of heavy charged particles in polycrystal. JETP **99**, 958 (2004)
6. Shevelko, V.P., Tolstikhina, I.Y., Stolker, T.: Stripping of fast heavy low-charged ions in gaseous targets. NIM B **184**, 295 (2001)
7. Ishii, K., Morita, S.: Continuum x-ray produced by light-ion-atom collisions. Phys. Rev. A **30**, 2278 (1984)
8. Sonnichsen, C.: Plasmons in Metal Nanostructures. Cuvillier Verlag, Gottingen (2001)
9. Tsytovich, V.N., Oiringel, I.M. (eds.): Polarization Bremsstrahlung. Plenum, New York (1991)
10. Grishin, V.K.: Vestnik MGU **2**, 69 (2004) (in Russian)
11. Astapenko, V.A., Gostishev, N.A., Zhukova, P.N., Nasonov, N.N., et al.: Modification of the EDXD method for diagnostics of polycrystalline and fine-grained media. Bull. Russ. Acad Sci. Phys. **72**, 863 (2008)

12. Korol', A.V., Lyalin, A.G., Obolenskiy, O.I., Solov'ev, A.V.: The role of the polarization mechanism for emission of radiation by atoms over a broad photon frequency range. JETP **87**, 251 (1998)
13. Van de Hulst, H.C.: Light Scattering by Small Particle. Dover, New York (1981)
14. Ter-Mikaelian, M.: High Energy Electromagnetic Processes in Condensed Media. Wiley, New York (1972)
15. Shevelko, V.P., Tolstikhina, I.Y., Stolker, T.: Stripping of fast heavy low-charged ions in gaseous targets. Nucl. Instrum. Methods Phys. Res. B **184**, 295 (2001)
16. Berestetskii, V.B., Lifshitz, E.M., Pitaevskii, L.P.: Quantum Electrodynamics. Elsevier, Oxford (1982)